

OFFICIAL FILE COPY

AFWAL-TR-80-4045

ADA 087927

MECHANICAL PROPERTIES VS. MORPHOLOGY OF ORDERED POLYMERS

E. L. THOMAS

R. J. FARRIS

S. L. HSU

MAY 1980

TECHNICAL REPORT AFWAL-TR-80-4045

1 September 1978 — 30 August 1979

Approved for public release; distribution unlimited.

MATERIALS LABORATORY
AIR FORCE WRIGHT AERONAUTICAL LABORATORIES
AIR FORCE SYSTEMS COMMAND
WRIGHT-PATTERSON AIR FORCE BASE, OHIO 45433

20040226202

BEST AVAILABLE COPY

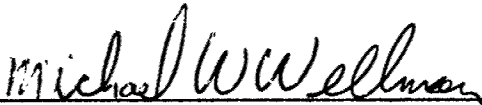
OFFICIAL FILE COPY

NOTICE

When Government drawings, specifications, or other data are used for any purpose other than in connection with a definitely related Government procurement operation, the United States Government thereby incurs no responsibility nor any obligation whatsoever; and the fact that the government may have formulated, furnished, or in any way supplied the said drawings, specifications, or other data, is not to be regarded by implication or otherwise as in any manner licensing the holder or any other person or corporation, or conveying any rights or permission to manufacture use, or sell any patented invention that may in any way be related thereto.

This report has been reviewed by the Office of Public Affairs (ASD/PA) and is releasable to the National Technical Information Service (NTIS). At NTIS, it will be available to the general public, including foreign nations.

This technical report has been reviewed and is approved for publication.



M. W. WELLMAN, Project Scientist
Polymer Branch



R. L. VAN DEUSEN, Chief
Polymer Branch

FOR THE COMMANDER



F. D. CHERRY, Chief
Nonmetallic Materials Division

"If your address has changed, if you wish to be removed from our mailing list; or if the addressee is no longer employed by your organization please notify AFWAL/MLBP, W-PAFB, OH 45433 to help us maintain a current mailing list"

Copies of this report should not be returned unless return is required by security considerations, contractual obligations, or notice on a specific document.

REPORT DOCUMENTATION PAGE		READ INSTRUCTIONS BEFORE COMPLETING FORM
1. REPORT NUMBER AFWAL-TR-80-4045	2. GOVT ACCESSION NO.	3. RECIPIENT'S CATALOG NUMBER
4. TITLE (and Subtitle) Mechanical Properties vs Morphology of Ordered Polymers		5. TYPE OF REPORT & PERIOD COVERED End of first year effort 1 Sep 1978 - 30 Aug 1979
		6. PERFORMING ORG. REPORT NUMBER
7. AUTHOR(s) E. L. Thomas, R. J. Farris and S. L. Hsu		8. CONTRACT OR GRANT NUMBER(s) F33615-78-C-5175
9. PERFORMING ORGANIZATION NAME AND ADDRESS Polymer Science & Engineering Department The University of Massachusetts Amherst, Massachusetts 01003		10. PROGRAM ELEMENT, PROJECT, TASK AREA & WORK UNIT NUMBERS
11. CONTROLLING OFFICE NAME AND ADDRESS Materials Laboratory Air Force Wright Aeronautical Laboratories Air Force Systems Command Wright-Patterson Air Force Base, OH 45433		12. REPORT DATE May 1980
14. MONITORING AGENCY NAME & ADDRESS (if different from Controlling Office)		13. NUMBER OF PAGES
		15. SECURITY CLASS. (of this report)
		15a. DECLASSIFICATION/DOWNGRADING SCHEDULE
16. DISTRIBUTION STATEMENT (of this Report) Approved for public release; distribution unlimited.		
17. DISTRIBUTION STATEMENT (of the abstract entered in Block 20, if different from Report)		
18. SUPPLEMENTARY NOTES		
19. KEY WORDS (Continue on reverse side if necessary and identify by block number) Heterocyclic Polymers Rodlike Polymers High Modulus High Strength		
20. ABSTRACT (Continue on reverse side if necessary and identify by block number) Morphological techniques in conjunction with mechanical testing have been employed to determine the relationships between mechanical properties and morphology of a new class of high strength, high modulus, thermally stable aromatic heterocyclic polymers. The polymers studied were poly-p-phenylene benzobisoxazole (PBO) and predominantly poly-p-phenylene benzobisthiazole (PBT). The microstructural studies involved laser Raman and Fourier transform infrared spectroscopy, electron diffraction and electron microscopy, wide and small angle		

x-ray scattering and birefringence measurements. Mechanical measurements have employed ambient and high temperature mechanical testing as a function of strain rate and state of stress (uniaxial tension, double loop bending).

The effect of processing conditions on fiber morphology and subsequently on mechanical properties has been studied for optimization of processing conditions for high strength and modulus rigid rod polymer fibers and films.

FOREWORD

This report covers the work performed by the University of Massachusetts, Amherst, Massachusetts 01003, on "Mechanical Properties versus Morphology of Ordered Polymers". The work was conducted under contract F33615-78-C-5175 for the Materials Laboratory. The performance period was from 1 September 1978 to 1 September 1979. This report was submitted in November 1979.

The work was performed in the Polymer Science and Engineering Department with Dr. Edwin L. Thomas acting as principal investigator. Authors of this report are E. L. Thomas, S. L. Hsu and R. J. Farris. The assistance of Drs. E. Roche, P. Shu, T. Takahashi and A. Kulshreshtha and Messrs. A. Filippov, S. Allen and J. Minter is gratefully acknowledged. The project engineer was Captain Michael W. Wellman, AFWAL/MLBP, Materials Laboratory, Wright-Patterson Air Force Base, Ohio.

TABLE OF CONTENTS

Section 1	OVERVIEW	1
Section 2	SPECTROSCOPY	9
	2.1 Introduction	9
	2.2 Experimental	10
	2.3 Data Analysis Computer Programs	12
	2.4 Chain Conformation	12
	2.5 Protonation Effects	13
	2.6 Degradation	16
	2.7 Articulated Polymers	17
Section 3	MICROSTRUCTURE	30
	3.1 Introduction	30
	3.2 Optical Microscopy	31
	3.3 Fiber Diameters	32
	3.4 Birefringence of Fibers	33
	3.5 Theoretical Calculation of Refractive Index	34
	3.6 X-Ray Diffraction of Fibers	36
	3.7 Radiation Damage	37
	3.8 Electron Diffraction	38

3.9	Analysis of the Broadening of (00 ℓ) Electron Diffraction Lines	41
3.10	Small Angle X-Ray Scattering of Fibers	43
3.11	Electron Microscopy	43
3.12	Dark Field Electron Microscopy	44
3.13	Structure of Coagulated Films	46
Section 4	MECHANICAL PROPERTIES	65
4.1	Introduction	65
4.2	Comments on Fiber Defects	65
4.3	Gauge Length Study	66
4.4	Fiber Morphology Summary	67
4.5	Environmental Effects	68
4.6	Heat Treatment	69
4.7	Tensile Properties	69
4.8	Bending Properties	71

LIST OF ILLUSTRATIONS

Figure		Page
2.1	UV Spectra of PBO in MSA	22
2.2	UV Spectra of PBT in MSA	23
2.3	Laser-Raman Spectra of PBO in MSA.	24
2.4	Laser-Raman Spectra of PBT in MSA.	25
2.5	FTIR Spectra of PBO.	26
2.6	Laser Raman Spectra of trans-PBT Model Compound.	27
2.7	Laser Raman Spectra of trans-PBO Model Compound.	28
2.8	Laser Raman Spectra of cis-PBT Model Compound.	29
3.1	% MSA in Coagulant	51
3.2	Zero Level Precession X-ray Photograph of PBT (CMU 53-46). Fiber Axis Vertical.	52
3.3	Electron Diffraction Patterns from Fibrillar Fragments of A PBT Fiber Exhibiting Different Degrees of Order.	53
3.4	Possible Unit Cells of the PBT Crystal Structure (projection down the c axis).	54
3.5	Schematic of the Proposed Arrangement of PBT Molecules In a Crystallite	55
3.6	Flat Film X-ray of Fiber 53-46 (courtesy of Dr. D. Wiff, UDRI).	56
3.7	Plot of Integral Breadth $\delta\beta$ Against the Square of the Order of Reflection.	57
3.8	Scanning Electron Micrograph of a Partially Peeled PBT Fiber . .	58
3.9	Equatorial Dark Field Image of a Fragment of a PBT Fiber	59

Figure		Page
3.10	BF (left) and DF (right) Images of Ribbon-Like Fragments of a PBT Fiber Showing the Fibrillar Texture Of the Ribbons	60
3.11	Electron Micrograph Showing Orientation Effects on the Banded Structure	61
3.12	Schematic of the Fibrillar Structure of the Ribbon-Like Fragments Obtained After Peeling and Mild Sonication of PBT Fibers	62
3.13	Bright Field TEM Micrograph of PBO Coagulated in Methanol At Room Temperature	63
3.14	Oriented Film of PBT Coagulated from 100% H ₂ O.	64
4.1	SEM Micrograph of a PBT 5348 Fiber. Arrows Indicate Characteristic Circumferential Bands.	75
4.2	PBT 5348, SEM Micrograph Showing a Longitudinal Depression . .	76
4.3	The Effect of Heat Treatment Time in a 175°C Oven on The Strain at Break of a PBT 9-3 Fiber	77
4.4	Effect of Heat Treatment Temperature on the Stress-Strain Curve of PBT Fiber	78
4.5	Comparison of the Stress-Strain Behavior of Fibers Heat Treated with and without Oxygen Present During Heat Treatment.	79
4.6	Tensile Behavior of PBT Fiber.	80
4.7	Strain Rate Independent Behavior	81
4.8	Analysis of Fiber Bending.	82
4.9	Fiber Loop Efficiency.	83

LIST OF TABLES

Table		Page
1.1	PBT Fiber Samples	8
2.1	UV-Visible λ_{max} In nm	19
2.2	Laser-Raman Spectra of Model Compounds Bands Peaks in cm^{-1}	20
2.3	Model Compounds (articulated)	21
3.1	Defects in PBT-27554-#	48
3.2	Fiber Diameter.	48
3.3	Radiation Resistance of Selected Polymers	49
3.4	Relative Intensities of 00 ℓ Reflections	50
3.5	Integral Line Breadths for 00 ℓ Reflections.	50
4.1	Mechanical Test Data.	74

SECTION 1: OVERVIEW

The goal of our work this past year has been to use morphological techniques in conjunction with mechanical testing to determine the relationships between mechanical properties and morphology of a new class of high strength, high modulus, thermally stable aromatic heterocyclic polymers. Fibers have been successfully spun at Carnegie-Mellon University and Celanese Research Corporation using a dry jet-wet spin process from liquid crystalline solutions. The polymers studied were poly-p-phenylene benzobisoxazole (PBO) and predominantly poly-p-phenylene benzobisthiazole (PBT). The microstructural studies involved laser Raman and Fourier transform infrared spectroscopy, electron diffraction and electron microscopy, wide and small angle x-ray scattering and birefringence measurements. Mechanical measurements have employed ambient and high temperature mechanical testing as a function of strain rate and state of stress (uniaxial tension, double loop bending).

The effect of processing conditions on fiber morphology and subsequently on mechanical properties has also received considerable attention with feedback to Celanese to assist in their optimization of processing conditions for rigid rod polymers. The overall goal of our work is to determine the relationships between mechanical properties of rigid rod polymer fibers and films with their microstructures. We have undertaken three general approaches to this end:

1. Spectroscopic Studies (see Section 2: Dr. S.L. Hsu),
2. Microstructure Studies (see Section 3: Drs. E.L. Thomas, R.S. Stein),

3. Mechanical Studies (see Section 4: Dr. R.J. Farris).

We have been supplied with fiber from Carnegie-Mellon University and Celanese Research Corporation. Unprocessed polymer has been received from Stanford Research Institute (see Sample Inventory - Table I).

Spectroscopic Studies

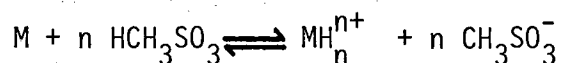
Professor Hsu's state of the art FTIR and laser Raman equipment has provided key data on solution and solid state polymer conformation. With the cooperation of Dr. Evers at WPAFB the model compound studies are leading to additional understanding of protonation and degradation effects. There is a good tie-in with Professor Berry's work at Carnegie-Mellon University on protonation. Spectroscopic studies are also of extreme importance with respect to polymer processing because of the prolonged times at elevated temperatures.

Our spectroscopic studies are directed towards a better understanding of the chain conformation and chain packing associated with these high modulus fibers. Our studies in the past year have raised several interesting questions. We feel the answers to these questions will complement other characterization techniques to elucidate the structure-property relationship for the high modulus materia. Fruitful research areas we foresee include:

1. Protonation Effect
2. Chain-Chain Interaction
3. Swivel Polymers
4. Degradation Effects

In the first area of study, as expected, we have evidence showing the polymers in solution exist in the protonated form. Model compounds have

proven to be extremely helpful in this study, because they can be dissolved in non-protonic solvent such as chloroform, or in strong acid such as MSA or CSA. We have qualitatively analyzed the spectral changes which occurred when model compounds dissolved in various solvents. For example, we found the



group is not highly protonated for trans or cis PBT model compound. In contrast, because of the oxygen, trans or cis PBO model compound is very sensitive to solvent interaction. These changes can be observed in UV-visible absorption and Raman spectra. Quantitative assignments for the vibration observed and their changes may elucidate the protonation effect for these polymers.

The second area of study includes the non-bonded chain-chain interaction in the solid state. It is known the unit cell associated with the model compounds cannot be directly transferable to the polymer. However, the models do display explicit evidence of well defined non-bonded molecular interaction. There are vibrations which are highly sensitive to temperature (77°K - 273°K). These bands occur in the very low frequency region of the Raman spectra. We have assigned these particular bands to the rotatory motions of the molecules in the unit cell. The non-bonded interaction (such as D.E. Williams potential) can and should be incorporated into our analysis of the vibrational spectra. These studies will answer questions regarding the specificity and magnitude of the molecular interaction. This type of information directly leads to the ideal strength achievable for these PBO or PBT's.

We have developed the multivariant statistical technique to examine the most minute interactions between the units on the chain that include the PBO

and the swivel linkages. We know the intrinsic viscosity of these polymers even with very low swivel concentrations is lower than neat PBO's. The changes in the interactions along the chain for polymers in solution compared to the solid state gives a better understanding of chain conformation and also contributes to a better understanding of the degree of chain extension.

In the last area of study, we plan to develop new spectroscopic techniques to follow the thermal degradation. The UV-visible absorptions have shown the polymer in solution rapidly decomposes to monomer when exposed to heat. We wish to carefully identify the degraded products. We plan to construct the external reflectance unit to follow the degradation of the polymer in the solid state. As mentioned previously, because of protonation, the degradation mechanism may be completely different for polymers in the solution versus polymers in the solid state.

Morphological Studies

We have made good progress, especially with the aid of microarea electron diffraction in studying the structure of crystalline PBT. Specimen preparation techniques, always the key to any microscopic study, are now well established and a large number of fibers with different processing histories are being examined. A cooperation this past year with Professor L. Azaroff of the University of Connecticut lead to an initial model for the structure of PBT fibers. The collaboration of another visiting scientist, Dr. E. Roche of Grenoble, France, has lead to an improved model of PBT crystal structure and hopefully with optimally processed and heat treated fiber a complete structure analysis (x_i, y_i, z_i) of PBT can be worked out.

Dr. Takahashi's dark field microscopy shows a banding along the fiber

axis very similar to that observed in PPTA fibers. His radiation damage studies indicate a fair chance of achieving lattice resolution. This powerful technique allows direct visualization of the atomic scale structure of the PBT crystals. Only Professor Johnson's group at the University of Leeds, United Kingdom, has achieved lattice resolution (of PPTA). With the somewhat better radiation stability of PBT over PPTA, we may be able to study defects within the crystals, much as is done with metallic and ceramic materials. The technique of microarea electron diffraction has enabled us to distinguish local variation in degree of order along and across fibers. We have recently purchased a diamond microtome knife and plan longitudinal and transverse sectioning to examine PBT fibers for the skin-core morphology indicated from the electron diffraction, mechanical and fracture surface studies.

The measurement of fiber birefringence, usually quite straightforward for melt spun fibers, has been a challenge for PBT. We have tried several methods and all have thus far failed, apparently due to the extremely high indices of refraction of the fiber. We are now working with very high index immersion liquids using the Becke line method. The optical properties of the fibers indicate the likelihood of strong internal field effects.

Finally, we have received approval from Oak Ridge National Laboratory for a small angle neutron scattering study on PBT. Determinations of the radius of gyration (R_G) and of chain length (L) [rod scattering theory gives the mass per unit length ($M/2L$)] will permit actual assessment of the rigidity of the molecules in the different samples and will provide a useful comparison to Professor Berry's solution light scattering studies. In addition, with a two dimensional position sensitive detector, we will have a quantitative measure of the fiber orientation which can be compared with our

wide angle x-ray data.

Mechanical Studies

The surprising nonlinear stress-strain behavior of the as-spun fiber has been tentatively interpreted as due to internal stresses from fiber spinning. We plan to pursue the investigation of internal stress in the fiber by annealing as spun fibers with and without fixed ends and by local heating of the fiber. We still seek to determine strength of void free fiber. The most recent results on Celanese heat treated fiber, 1600 g/d modulus, 16 g/d tenacity, are indeed very promising, however, fracture surface studies indicate flaws still control fiber failure and we are not yet realizing the intrinsic fiber strength. Prompted by initial observations of deformation (shear) bands on fibers wound on small diameter take-up reels at Carnegie-Mellon University, Filippov developed fiber bending tests which reveal information on compressive strength and susceptibility of the fiber to buckling failure.

A servohydraulic Instron Tester equipped with an environmental chamber and special load transducers is used for fiber studies. The programmability of the instrument allows for detailed deformation history studies including fatigue studies as a function of amplitude, frequency and temperature. Preliminary data indicate that even the highly flawed fibers have excellent fatigue properties, requiring on the order of 10^6 to 10^7 cycles at a high fraction of ultimate strength to cause failure. The failure in fatigue is much more fibrillar than that experienced with simple tension tests and suggests a different failure mechanism, perhaps an interlaminar shear type failure.

Heat treatment data indicates a loss in plasticity of the fibers, perhaps due to the experienced weight loss during heat treatment. Identification of the mechanism of plasticity would be important and could shed considerable light on the deformation mechanisms in these rigid rod materials. The topic of plasticity is currently being investigated and because of its importance will be a topic of research until the mechanisms are identified.

This report is organized along the lines of the these three general experimental program areas. Our ultimate goal is to obtain as detailed as possible a mechanical and morphological picture of the films and fibers, both as spun and deformed. Some preliminary morphology-property relations are evident at this stage of the work and are given in the appropriate sections. Further in depth studies are required before final correlation and modeling can synthesize an overall understanding of the processing - microstructure - mechanical property relations for these materials.

TABLE 1.1: PBT FIBER SAMPLES

Carnegie-Mellon: Samples spun with MSA as solvent.

Sample Designation	Polymer	Fiber Funnished	Coagulation Conditions
Series 53	IV 18	13 samples	50/50 methanol/sulfolane Room Temperature
Series 62	IV26	18 samples	

Celanese: Samples spun from 97.5% MSA, 2.5% CSA solution.

Sample Designation	Polymer	Fiber Funnished	Coagulation Conditions
Series 27554-6	IV 14	3 samples	25-37.5-50 MSA/H ₂ O Room Temperature
27554-9	IV 18	8 samples	
27554-24	IV 18	9 samples	50/50 MSA/H ₂ O, 23°C; 8°C
27554-27	IV 18	only short samples	50/50 MSA/H ₂ O, -10°C; 23°C
27554-33	IV 18	7 samples	50/50 MSA/H ₂ O, 24°C; 7°C

SECTION 2: SPECTROSCOPY

2.1 Introduction

Vibrational studies of PBO, PBT, and their model compounds have been carried out in order to elucidate more fully the features of morphology at the microstructural level. It is important to determine the degree of chain extension, chain rigidity and chain-chain interaction in the solution and solid states in order to help determine the ultimate strength and modulus associated with these materials. In addition, we are interested in identifying the mechanism of degradation and the degraded products.

The source of information available to vibrational spectroscopy includes band position, band intensity, band shape and dynamic measurements of their changes. Experimental studies, in conjunction with normal mode vibrational calculations, should provide qualitative and quantitative explanations of features sensitive to changes in the secondary structure of polymers.

With the exception of poly-p-phenylene terephthalamide (PPTA) (Kevlar), there are relatively few spectroscopic studies directed at the microstructure of high modulus fibers⁽¹⁾ However, there are a number of investigations directed at the chain conformation and packing of conjugated polymers⁽²⁻⁴⁾. These studies may contribute a better estimate of the theoretical modulus and strength of crystalline polymers, including aromatic polyamides⁽⁵⁾.

Because of the conjugated backbone structure associated with PBO and PBT, strong resonance enhancement is expected in the Raman scattering intensities for the vibrational motions coupled to the electronic transitions of the backbone. The optical activities of these motions are highly dependent on the local symmetry properties associated with chain conformation and packing. The vibrational and absorption spectra, if properly interpreted, may be used to

understand the degree of rigidity (resonance structure) and the magnitude of fiber strength (interchain interaction).

We have examined PBO and PBT in the solid and solution states. Furthermore, vibrational spectra of highly crystalline model compounds revealed structural information and nonbonded chain-chain interactions in the unit cell. In addition, a number of computer programs were written to analyze the intramolecular and intermolecular (lattice) motions.

2.2 Experimental

All of the vibrational spectroscopic studies were carried out on the Nicolet Fourier Infrared Spectrometer and the Jobin Yvon HG 2S Raman spectrometer. In addition, we have obtained ultraviolet (UV) and visible spectra on a Beckman Model V spectrometer.

The results of the UV/visible spectroscopy will be particularly pertinent in the selection of the minimum wavelength of radiation for resonance Raman spectroscopy. UV visible absorption spectra obtained for PBO and PBT in solid and solution are shown in Figures 2.1 and 2.2, respectively. Methane sulfonic acid (MSA), a solvent for these materials, was distilled under vacuum from a commercial source (Eastman). These absorption spectra of PBT display a number of sharp electronic transitions at 212(w), 268(m), 323(w), 426(s) and 441 (s) nm. PBO showed a number of transitions at 246(w), 306(w), 380(vw) 403(s) and 428 (s) nm. These absorptions are characteristic of the highly conjugated groups.

Extreme caution was exercised in preventing moisture from entering the sample solution by obtaining spectra from solution in the sealed preparation volumetric flasks.

As expected for these highly conjugated polymers, we saw strong Raman resonance enhancement for the vibrational motions coupled to the electronic structure of the backbone. The optical activity of these selective vibrational motions are highly sensitive to the local symmetry. Unexpectedly, substantial differences in band intensity and position were observed for polymers in solution compared to polymers in the solid form. As is true in general for these samples, the fluorescence background is very high. A higher excitation frequency (wavelength 4579 Å) is used to take advantage of the Raman resonance enhancement.

The spectra associated with PBO and PBT are shown in Figures 2.3 and 2.4, respectively. The Raman spectra obtained from cast film (from MSA), spun fibers, and unprocessed fibers are essentially identical. Since PBO and PBT both absorb strongly in the 400 nm region, and may thermally degrade in the laser beam, Raman spectra were obtained by the front surface reflection method off a spinning sample with excitations by wavelengths ranging from 5145 Å to 4579 Å (Argon laser)⁽⁶⁾.

Infrared data generally have been taken from cast film on salt substrate or pressed KBr pellet. The latter method is favored since it was difficult to control the thickness of the film. In addition, infrared spectra can be taken with the attenuated total reflectance technique. A typical spectra from PBO is shown in Figure 2.5. From our experience most of the quantitative spectroscopic studies should be carried out using either the internal or external reflection technique.

2.3 Data Analysis Computer Programs

During the last year, a series of six normal vibrational computer programs have been written to analyze the vibrational spectrum of a finite molecule or polymer chain⁽⁷⁾. These programs provide the capability to analyze the intramolecular vibrational transitions and to incorporate the nonbonded interactions (π - π overlap) between molecules in the unit cell of a three-dimensional lattice. These programs are coded in FORTRAN, requiring at least 32K of memory. In addition, we found the multivariate statistical technique of analysis can be used to find the number of the independent components associated with a set of digitized vibrational spectroscopic data. This program can detect very small relative shifts or changes in intensity associated with the vibrational transitions. The program used on the FTIR 1180-Nicolet Computer has been written and successfully tested⁽⁸⁾. This program is coded in BASIC.

2.4 Chain Conformation

As shown in Figures 2.1 and 2.2, the absorption spectra of PBT display a number of sharp electronic transitions at 212 nm(w), 268(m), 323(m), 426(s) and 441(s). PBO showed a number of transitions at 246 nm(w), 306(w), 380(vw), 403(s) and 428(s). The main peaks in the 400 nm region observed for PBO and PBT suggest these polymers possess fairly highly conjugated groups. The transition energies are comparable to the ones observed in poly(phenylene oxide) and poly paraphenylene. The transitions associated for the trans and cis isomers of monomeric model compounds are shown in Table 2.1. The electronic transitions observed for a PBT "dimer" are 267 nm(w), 338(vw), and 404(s), very similar to the ones obtained for the polymer. However, the degree of charge delocalization is still limited. This conclusion is consistent with the x-ray results showing similar C-C bond length between the benzobisthiazole

or benzobisoxazole group and the phenylene ring. This bond length is measured to be 1.469 Å, a value between the 1.54 Å and 1.34 Å expected for a single bond and double C-C bond, respectively.

As shown in Figures 2.3 and 2.4, we found strong resonance enhancement associated with Raman scattering intensities for the vibrational motions coupled to the electronic structure of the backbone. Unexpectedly, we observed substantial differences in the relative intensity and positions for polymers in acid solution (MSA) compared to the polymers in the solid form. For example, the band near the 1600 cm^{-1} , assignable to C=C stretching, changes from 1610 cm^{-1} to 1605 cm^{-1} from solution to the solid state. Furthermore, the band near 1500 cm^{-1} assignable to C=N stretching changes from 1515 cm^{-1} to 1481 cm^{-1} . These changes were independent of polymer solution concentration (from 0.9 to 14%).

Such changes are inconsistent with the assumption that the chain conformation remains essentially identical in dilute solutions. The strong possibility exists that in strong acid such as MSA, the polymers take on an essentially protonated form therefore affecting the electronic and vibrational transitions.

2.5 Protonation Effects

PBT and PBO only dissolve in a few strong acids (MSA, CSA, PPA, H_2SO_4). The dissolution is essentially a result of protonation of the hetero atoms on the polymer backbone. This causes changes which affect the interchain interactions (van der Waals) sufficiently to facilitate the dispersion (dissolution) of the polymer packing in the solid (crystalline) state. The processing of these polymers involves dissociation in MSA at elevated temperature, spinning of the dope and then coagulation followed by neutralization and washing. Therefore

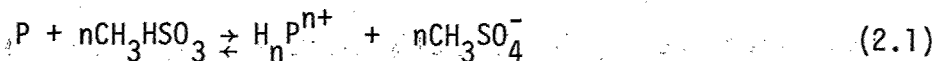
the investigation of the protonation effect and heating effects is very important to the understanding of the properties of the polymer solution as well as the resulting products.

As mentioned earlier, the concentration independent shift of C=N stretching band in laser Raman spectra from 1481 cm^{-1} (solid) to 1515 cm^{-1} (in MSA) may be a manifestation of the completely protonated polymers in MSA. The monomeric model compounds afford the advantage of being soluble in both CHCl_3 (a non-protonic polar solvent) and MSA, thus, the possible protonation effect for polymers in the solution state can be investigated by comparing the UV-visible and laser Raman spectra of the monomeric model compounds in the solid state and in CHCl_3 and MSA solutions.

Substantial differences are found for both band positions and relative intensities for those model compounds in the different solution and solid states. The spectra obtained are shown in Figures 2.6-2.8. The observed bands in the $1500\text{-}1600\text{ cm}^{-1}$ region are listed in Table 2.2.

As is shown in Table 2.2 and Figure 2.7, PBO model compounds similar to the PBO polymer showed substantial changes in the $1500\text{-}1600\text{ cm}^{-1}$ region (C=C and C=N stretching motions) when dissolved in MSA. In contrast, PBT model compounds showed relatively small changes when dissolved in MSA. In addition, spectra obtained for PBO and PBT model compounds in CHCl_3 , a non-protonic polar solvent, are quite similar to the solid state spectra. We have interpreted these spectral changes to be caused by the protonation effect.

The protonation process in MSA can be expressed by Equation 2.1:



where P represents polymers or model compounds and n denotes the number of protons being associated with P.

The electronegativities of the atoms of the backbone composition are:

O	N	C	S
3.50	3.07	2.50	2.44

where n equals 8 for each repeat unit⁽⁹⁾. The O and N atoms are most likely to be protonated in the case of PBO in the completely protonated species. In contrast, $n = 4$ if each N and O is protonated on one side or sharing each H^+ by two heteroatoms or adjacent chains. The electronegativity (or basicity) of S (2.44) is lower compared to O (2.50), therefore it should be less susceptible to protonation. Therefore, $n = 4$ (protonated on both sides) and $n = 2$ (protonated on one side or shared intermolecularly) may be the case for PBT.

UV-visible spectra of trans-PBO and cis-PBT also show an upward shift in the absorption maxima (λ_{max}). The interpretation of these changes is unclear at the present time.

The more drastic change induced by protonation on PBO than on PBT seems to indicate that the protonated PBO at elevated temperature (see degradation section 2.6) is more prone to degradation. This effect may be particularly important for long term aging under elevated temperature for PBO. Thus, a possible reason for the inferior mechanical properties of PBO fibers to that of PBT fibers may be the protonation effect during the processing. All the wet analytical measurements for the MSA (or CSA) dope are really measuring the properties of the protonated polymers instead of the virgin polymers.

There is no significant change found between the spectra of model t-PBO or t-PBT in $CHCl_3$ and in $CHCl_3/LiCl$. This could result from the rather limited solubility of $LiCl$ in $CHCl_3$. If some suitable solvent is found to dissolve both the model compounds and $LiCl$, cationization (similar to protonation effect) and/or ionic strength effects should lead to a better understanding of the residual proton within the fiber and

possible Na^+ effect due to the neutralization process*. Ultimately, the cations may function as interchain cross-links and yield favorable strengthening of the mechanical properties.

Our swelling studies of PBT fibers in HNO_3 and H_2SO_4 showed a substantial drop in mechanical properties. This again could result from protonation, possibly coupled with degradation.

Further studies such as degree of protonation, long term protonation effect (at elevated temperatures), possible degradation, reversibility of protonation effect upon coagulation, defects induced by residual acid, etc., are needed to understand the protonation effect on the processing.

2.6 Degradation

The indirect heating of 14% PBT (2122-72) in MSA by a gas-oxygen flame yielded a solid with metallic appearance which could not be studied with laser Raman spectroscopy. The heating of 1% PBT (2122-72) in MSA sealed in a pipet at 100°C for 42 hours did not show any change in laser Raman peaks (1515.1 cm^{-1} and 1608.4 cm^{-1} for heated sample compared to 1516.7 cm^{-1} and 1608.7 cm^{-1} for unheated sample). The same sample was again heated at 200°C for four days and showed no substantial change spectroscopically (1518.6 cm^{-1} and 1610.1 cm^{-1}) even though the color darkened toward red from the original greenish-yellow color.

The same sample when heated at 300°C for four days, first changed to a brown color and then to a black suspension. A second sample was heated at 250°C

* We have observed some NaHCO_3 or Na_2CO_3 (used in neutralization) on the PBT fiber surface by SEM [(Na) identified by x-ray microanalysis, C=O and bonds by IR].

and it changed to a brown color after two hours. Both these brown and black suspensions cannot be identified by Raman. The UV-visible absorption spectrum of the above sample showed absorption maxima at 236 (m) and 350 (m) nm. These values are close to the λ_{max} of monomeric trans-PBT model compound. The spectrum of the decomposed product mixture should be analyzed to elucidate the degradation mechanism. The study of degradation of these polymers may give some indication of the stability of the processing dope.

2.7 Articulated Polymers

Four samples of articulated PBO samples were received from Dr. Evers (AFWAL/MLBP). These polymers (36-292, 58-292, 59-292, 62-292 [see Table 2.3]) contain 3-25% concentration of phenylene oxide "swivel" linkages. From the intrinsic viscosity measurements, these "swivel" linkages do provide increased flexibility for the chain. Therefore, it is important to understand more fully the chain conformation associated with these polymers in the solution and solid states.

The UV-visible spectra of these articulated polymers in the solution state (MSA) show great similarity. A strong doublet is found at approximately 405 nm, shifted from the 430nm peaks in neat PBO. Although the position of this doublet remains constant, the relative intensity of the two components changes dramatically with "swivel" content. Even for polymer containing the lowest concentration of the phenylene oxide linkages (3%), the absorption spectra do not show the electronic spectrum associated with neat PBO. A protonation effect alone cannot explain our observation. Possible interaction between the "swivel" and PBO units may sufficiently perturb the structure to yield the transitions seen.

In order to support this hypothesis, we have used the multivariate statis-

tical techniques of factor analysis and the ratio method to seek independent contributions giving rise to the infrared spectra associated with all four samples. That is, we are interested in searching and characterizing the PBO segments, the "swivel" linkages and their interactions in these articulated polymers. This type of analysis has been effectively used to distinguish the amount of disordered packing from the usual orthorhombic packing associated with polyethylene⁽⁷⁾.

From these spectra, we found a number of spectral features associated with the "swivel" linkages only. For example, bands at 1221 and 1487 cm^{-1} are dependent on the "swivel" content and can be assigned to the asymmetric stretching associated with ϕ -O- ϕ and ring vibrations, respectively. However, it should be noted that these bands are quite localized and insensitive to chain conformation changes. In addition, we found evidence of an independent contribution to the spectra. These features are assignable to the interaction terms between the "swivel" linkages and PBO of the articulated polymers. As expected, this component only exists in the spectral region sensitive to changes in chain conformation (400-1000 cm^{-1}). In contrast for the high frequency region, e.g., CH stretching in the 3000 cm^{-1} region, this third contribution is not found, since CH stretching vibrations are independent of conformation. These features can be used to elucidate the conformation of the "articulated" polymers in the solution state.

TABLE 2.1: UV-VISIBLE λ_{\max} IN nm.

Model Compound	in CHCl_3	in MSA
Trans PBO	231 (w)	248 (w)
	326 (s)	337 (m)
	341 (vs)	350 (s)
	358 (s)	368 (m)
Trans PBT	247 (m)	256 (w)
	270 (vw)	266 (s)
	334 (s)	350.5 (vs)
	348 (s)	362 (m)
	364.5 (m)	
Cis PBT	235 (w)	219 (m)
	299.5 (s)	261 (m)
	340 (m)	294 (s)
	360 (w)	350 (vs)
		360 (m)

TABLE 2.2: LASER-RAMAN SPECTRA OF MODEL COMPOUNDS BAND PEAKS IN cm^{-1} .

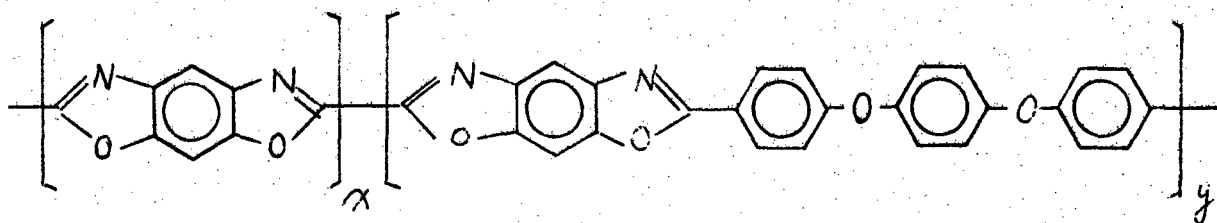
<u>Trans PBO</u>		<u>Cis PBT</u>	
in MSA	in CHCl_3	in MSA	in CHCl_3
1656.9 (VW)*	1655.4 (VW)*		
	1645.8 (VW)	1594 (S)*	1597.6 (M)*
1637.8 (M)*	1637.2 (VW)*	1524.3 (S)*	1526.0 (W)*
	1618.5 (S)	1491.1 (W)	1504.8 (S)
1602.0 (S)*	1602 (M)*	1437.3 (VW)	1482.3 (M)
		1348.6 (VW)*	1445.1 (W)*
1589.8 (M)*	1584.2 (M)*	1321.9 (VW,SW)	1416.1 (W)
	1562.5	1296.6 (S-M)	1271.- (W)
1577.1 (M)		1205.1 (VS)	1245.0 (W)
	1552.5 (VS)	1115 (VS)	1214.1 (W)
	1544.3 (Sh)	1110.9 (VW)*	1108.8 (W)*
		999.6 (W)	

* Denotes that no substantial change in peak position occurred.

TABLE 2.3: MODEL COMPOUNDS (ARTICULATED)

Sample No.	Structure	$\eta_{inh}(dl/g)^{(a)}$
36-292	$x = 0.75, y = 0.25$	2.34
58-292	$x = 0.90, y = 0.10$	3.18
59-292	$x = 0.95, y = 0.05$	3.57
62-292	$x = 0.97, y = 0.03$	6.75

(a) 25°C, 0.2 g/dl, MeSO₃H



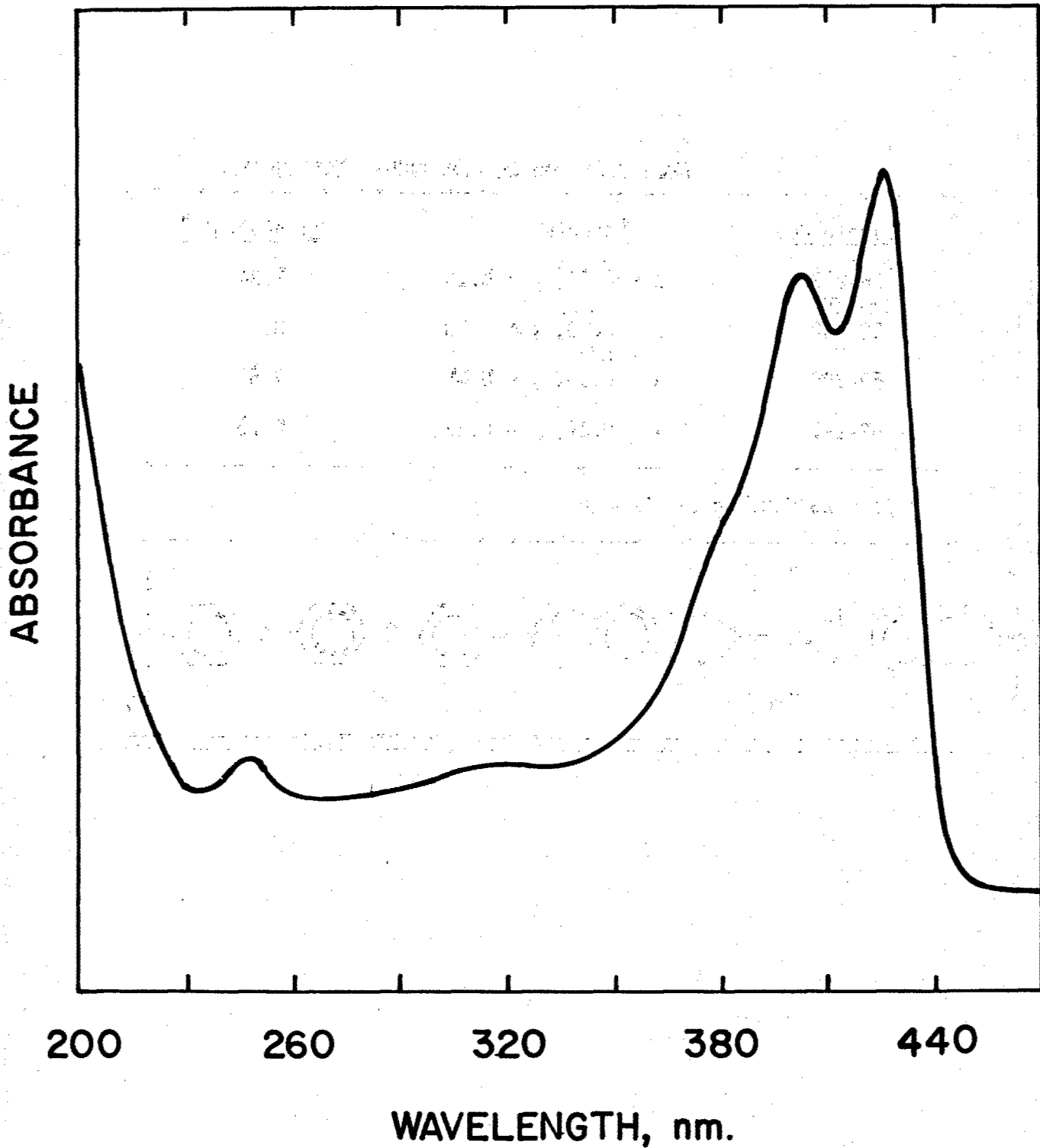


Figure 2.1: UV Spectra of PBO in MSA.

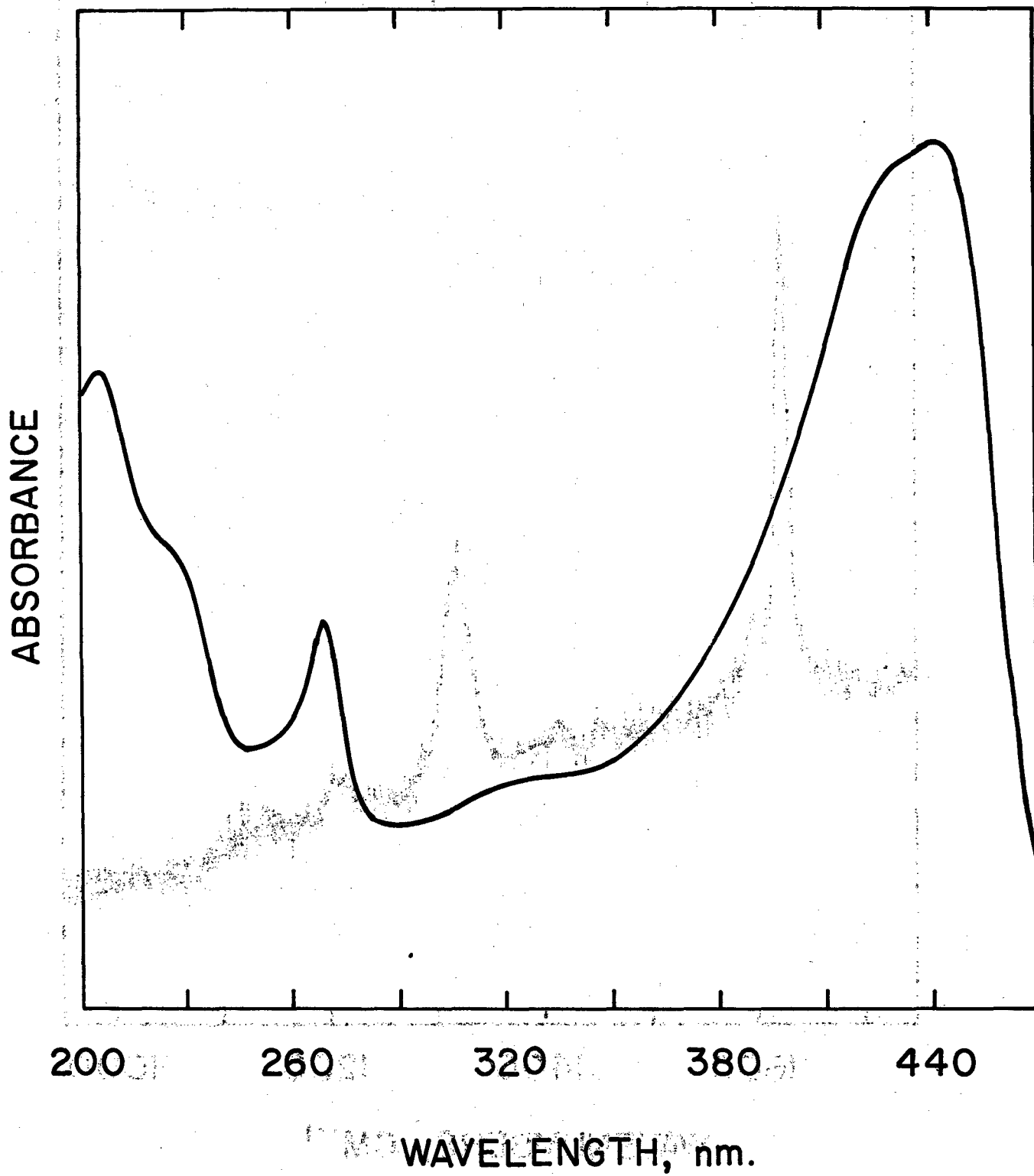


Figure 2.2: UV Spectra of PBT in MSA.

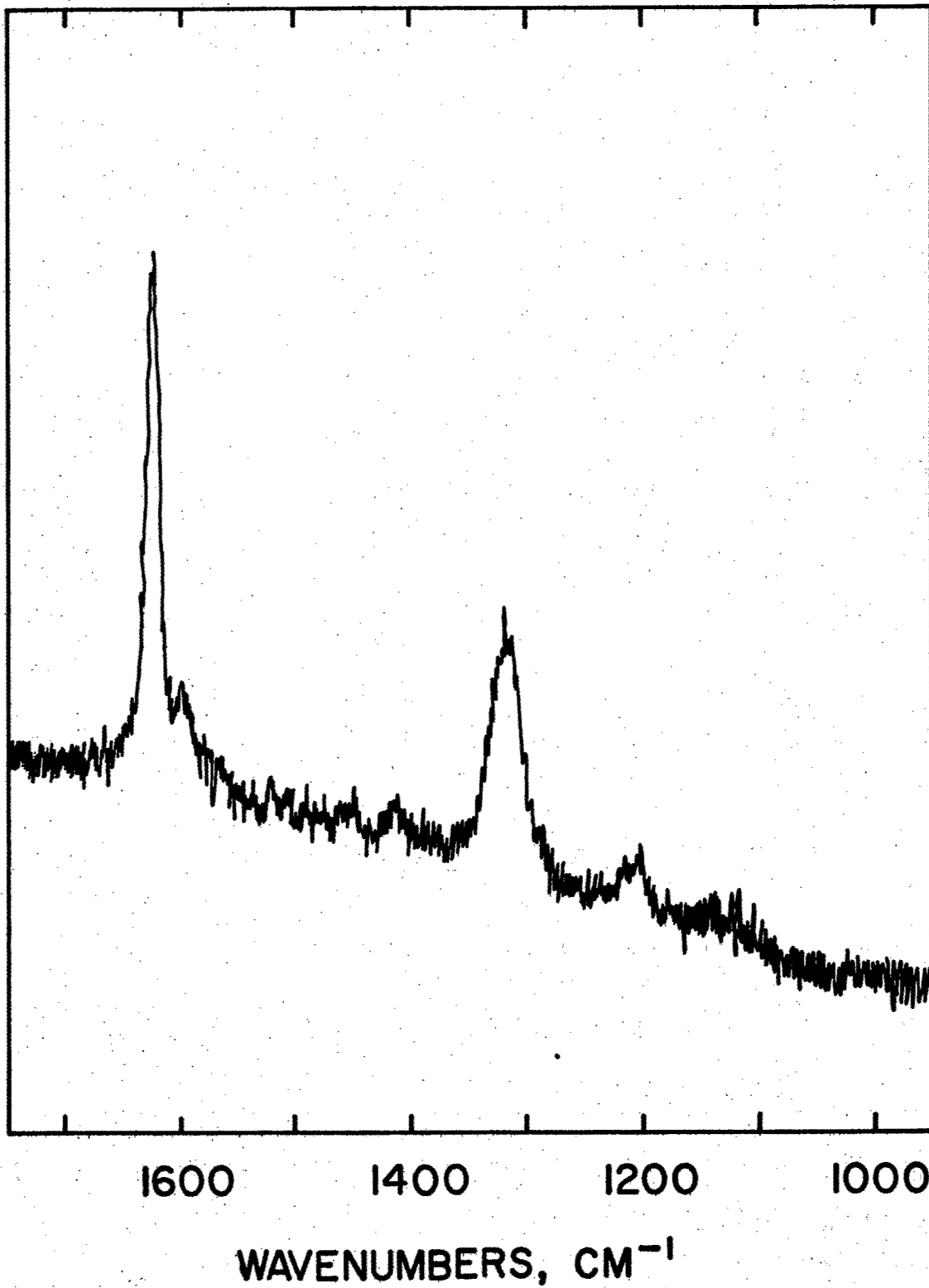


Figure 2.3: Laser-Raman Spectra of PBO in MSA.

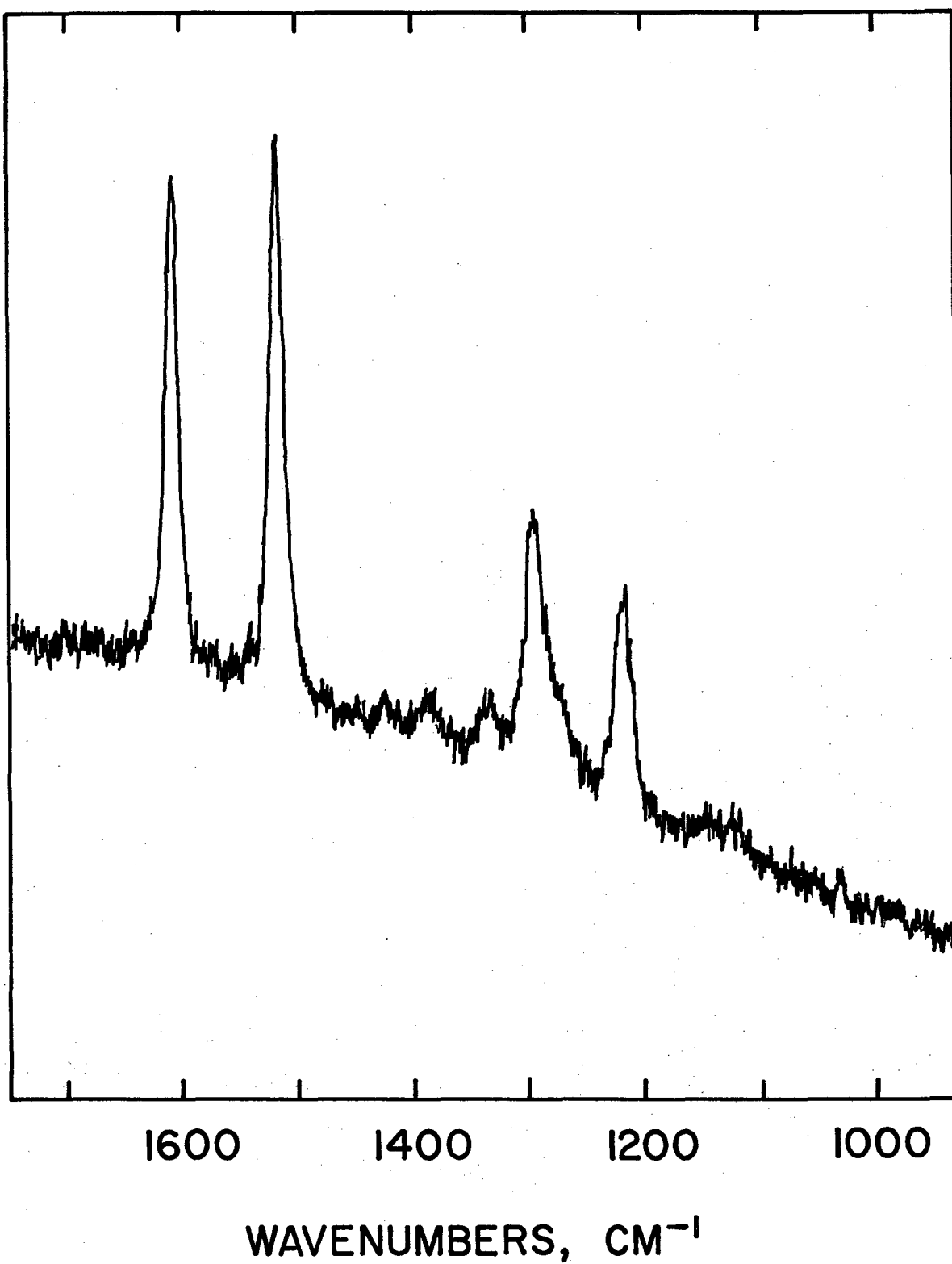


Figure 2.4: Laser-Raman Spectra of PBT in MSA.

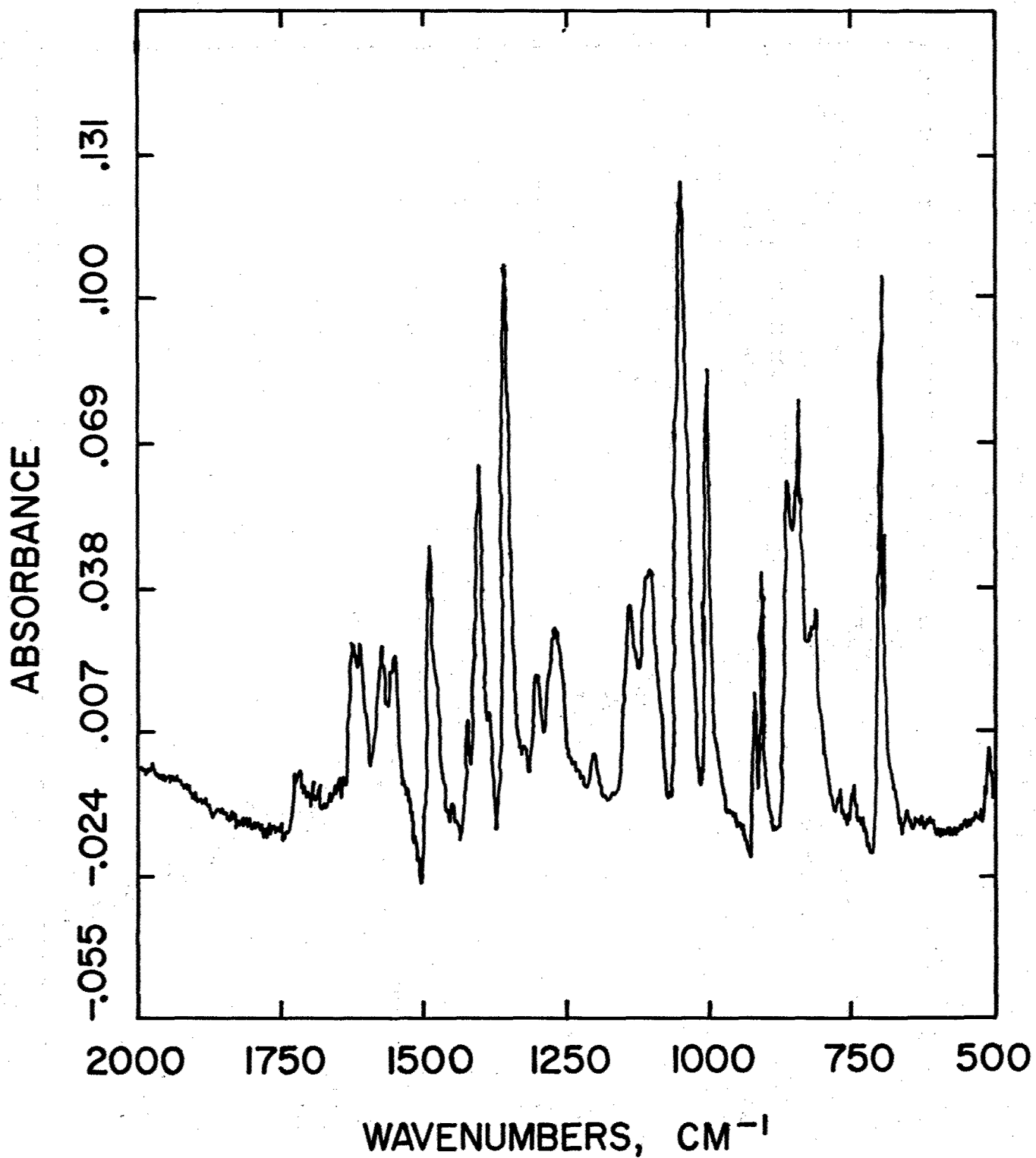


Figure 2.5: FTIR Spectra of PB0.

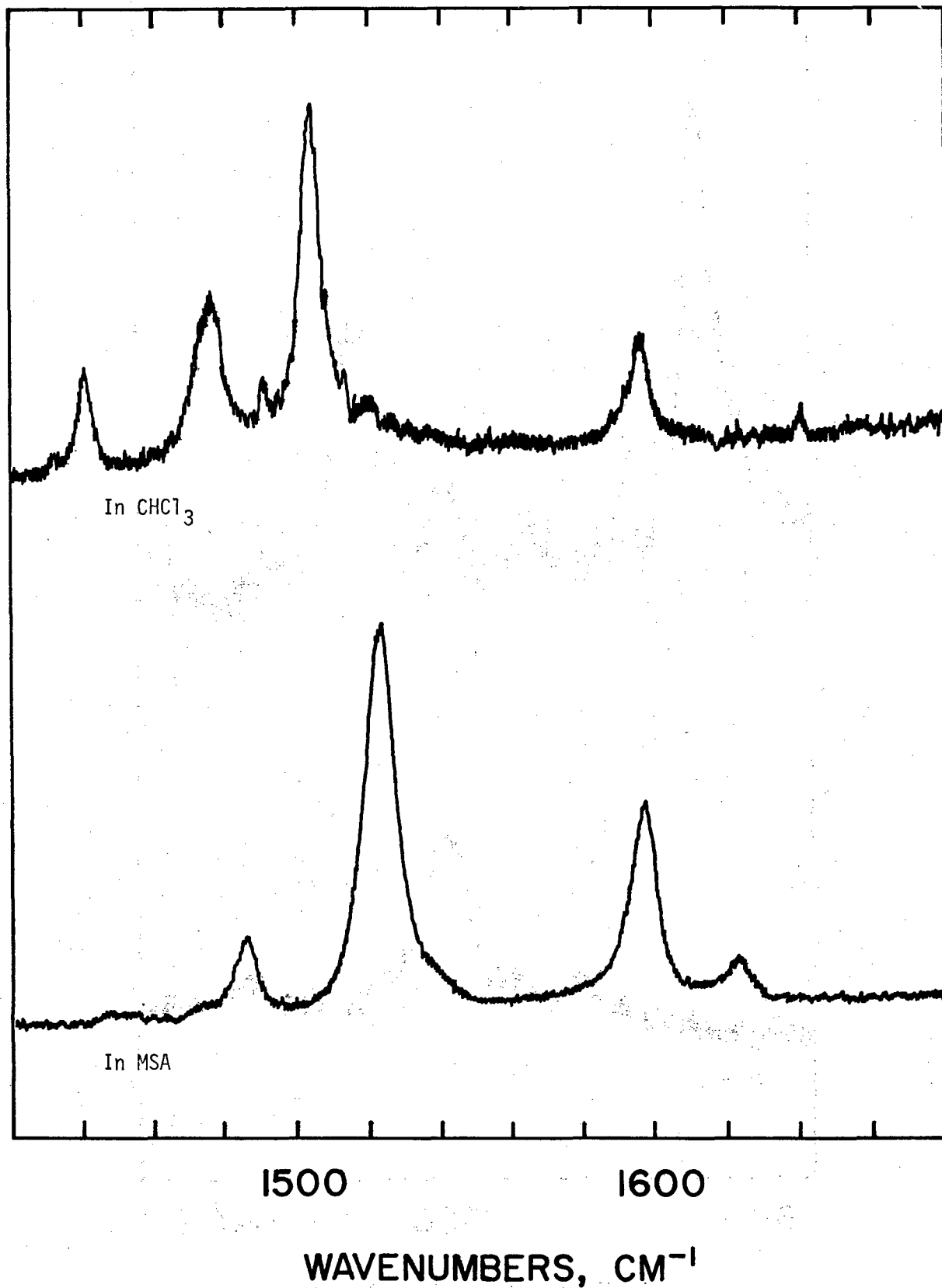


Figure 2.6: Laser Raman Spectra of trans-PBT model compound.

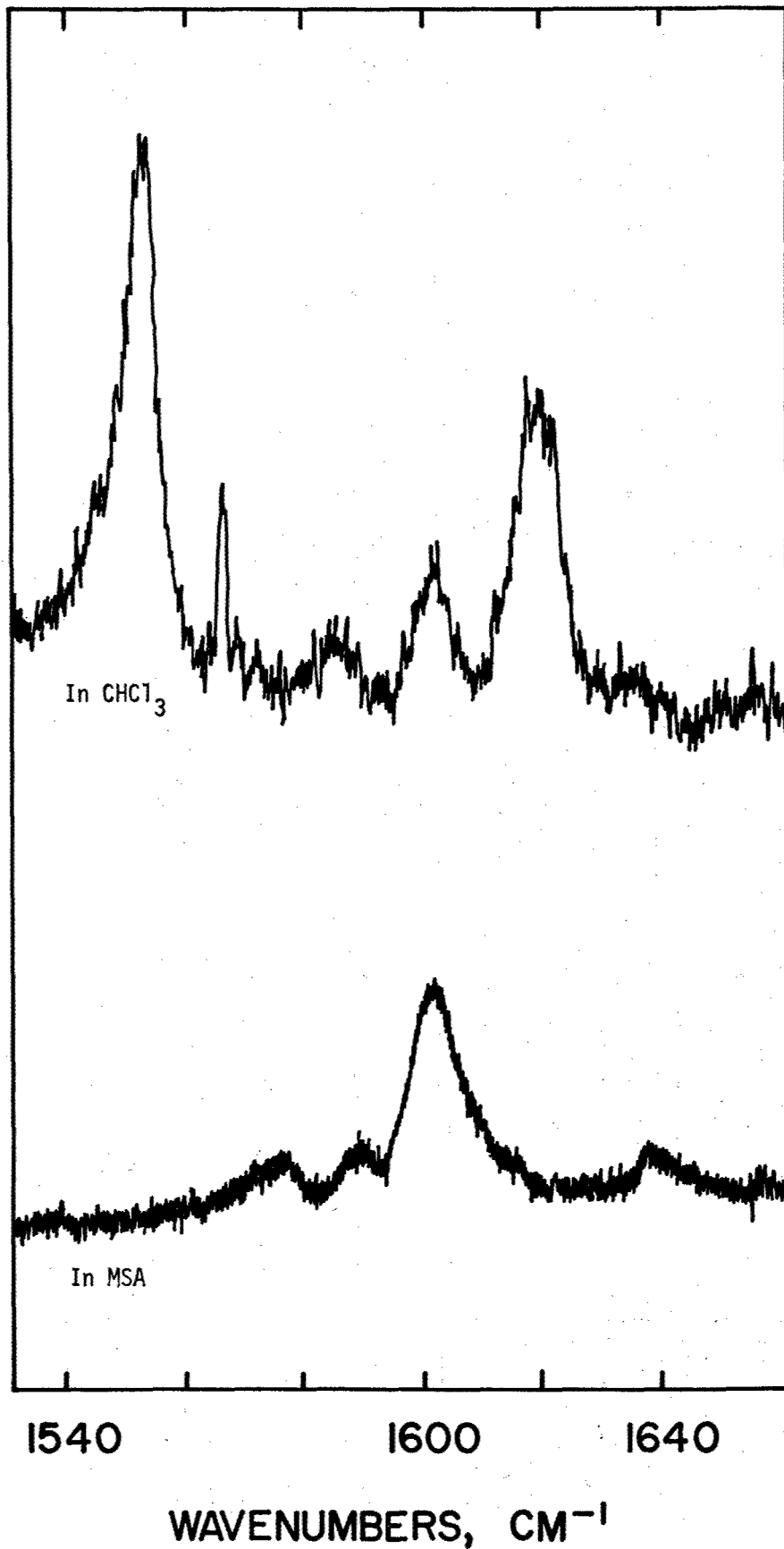


Figure 2.7: Laser Raman Spectra of trans-PBO model compound.

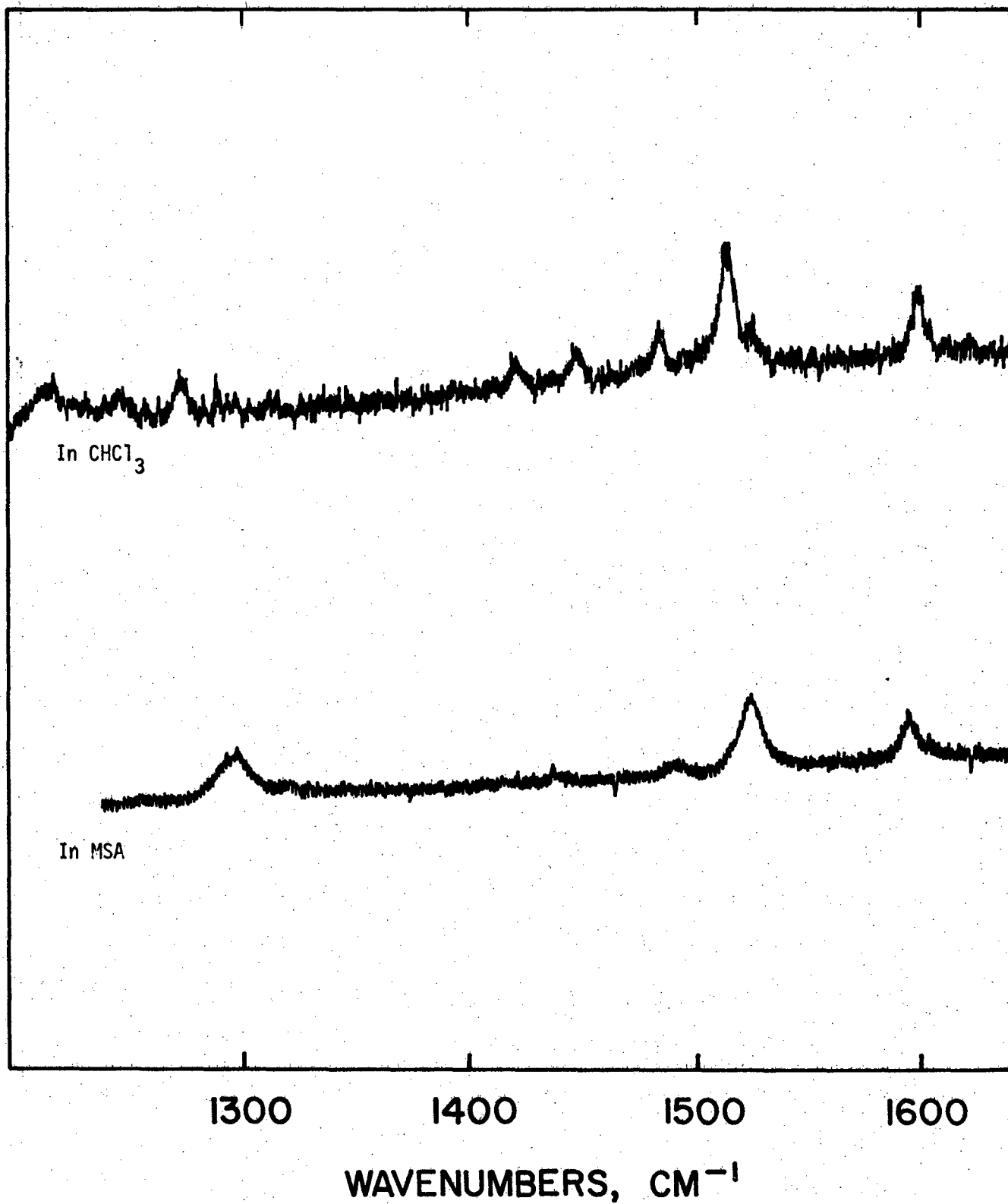


Figure 2.8: Laser Raman Spectra of cis-PBT model compound.

SECTION 3: MICROSTRUCTURE

3.1 Introduction

Our morphological studies have involved PBO and principally PBT and for comparative purposes PPTA (Kevlar) obtained from duPont. The fibers have various levels of structure. Optical microscopy and scanning electron microscopy have been used to examine the large scale features. We have found internal voids in the as spun fibers and conclusive fracture surface evidence that failure is initiated at these flaws. A radiation damage study on PBO and PBT indicates that these polymers are quite radiation resistant (better than PPTA) permitting high resolution electron microscopy studies and electron diffraction line breadth analyses. Molecular orientation, a key feature for high modulus and strength, has been examined by birefringence and x-ray and electron diffraction methods. The fibers are all highly axially oriented but the degree of lateral ordering of the chains depends on the fiber processing conditions. Combined x-ray and electron diffraction analysis suggests that PBT molecules can pack into a monoclinic unit cell. The calculated density is 1.69 which closely matches the observed fiber density of 1.6 for a fiber without macroscopic voids. Less ordered molecular arrangements also occur in the fiber. These regions appear as a "two-dimensional solid nematic phase" having characteristic broad equatorial reflections, meridional streaks and the absence of hkl-type reflections.

Bright field and dark field studies of the PBT fibers indicate a fibrous ribbon-like microstructure. Small elongated ($60 \times 300 \text{ \AA}$) crystallites are regularly distributed along the fibrils. In addition, fibril ribbons sometimes exhibit a wavy texture. The waviness or banding is regular with a periodicity of about 1200 \AA as compared to 5000 \AA for a similar banding observed in PPTA

fibers. The dark field results suggest each microfibril ribbon consists of a succession of narrow crystallites embedded in a somewhat less ordered matrix. Whether the banding appears due to sample preparation or is characteristic of the as spun fibers is not known at present. The non-linear stress-strain behavior and the elongation at break (see Section 4) suggest the bands may be shear bands. Whatever their origin, the bands reflect the susceptibility of the fibrils to transverse kinking or buckling.

Preliminary work on coagulated films of PBO and PBT has shown that in the absence of shear a "grassy" fibrillar mat is formed with 200 Å diameter fibrils. If the solution is sheared prior to coagulation, an oriented fibrillar film is produced. Such film samples are easily prepared and allow screening of coagulation-processing conditions. The effect of neutralization on the polymer has been studied by electron diffraction.

3.2 Optical Microscopy

A series of PBT fibers produced by Celanese has been examined under the optical microscope using approximately crossed polars and Zeiss-Nomarski differential interference illumination. In the "approximately crossed polars" technique the fiber is at 45° to the polarizer with the analyser at 77° to the polarizer. This gave improved contrast over the more usual technique where the analyser is 90° to the polarizer. Both techniques revealed that the fibers contain three principal types of defects which have been categorized as:

1. contained voids
2. erupted voids
3. circumferential bands.

The linear number density of these defects is given in Table 3.1. The only significant correlation of the defects with processing history is that the

largest number of voids (erupted voids) tended to decrease with increasing percentage of MSA in the coagulating bath (i.e., slower coagulation). This is shown in Figure 3.1. The circles represent inherent viscosity (IV) 18 polymer and the squares represent IV 14 polymer. Open points indicate that the fiber was coagulated at room temperature, filled points indicate that the fiber was coagulated at 8°C, and the half-filled point indicates that the fiber was coagulated with a 7°C bath followed by a room temperature bath (23°C) of identical composition.

These data suggest that further spinning runs, preferably on a small scale, will be necessary to achieve process optimization. The spinning parameters such as bath composition, draw-down ratio, residence time in the bath, bath temperature, polymer inherent viscosity, and spinnerette diameter must be varied in a systematic manner.

3.3 Fiber Diameters

Precision measurements of fiber diameter were performed on Celanese PBT fibers, using the laser light scattering method. For each sample of PBT fibers, five segments of filament were mounted parallel to each other on a microscopic glass slide (the ends of filament segments were fixed on the slide by an adhesive). Ten readings at different points along the fiber were obtained, giving a total of 50 measurements for calculating the mean fiber diameter. The standard deviation (S.D.) of fiber diameter, which is a measure of non-uniformity of fiber diameter, was also calculated (see Table 3.2).

3.4 Birefringence of Fibers

The optical anisotropy or birefringence provides a convenient measure of the extent of molecular alignment along the fiber axis. Sometimes fibers are not uniform in their molecular arrangement and the fiber birefringence varies over the cross-section. The elucidation of such inhomogeneity is of considerable practical importance in relating various physico-chemical properties of polymer fibers to the nature of the spinning and drawing operations.

In general, any anisotropic (crystalline) material has three principal refractive indices. However, fibers exhibit cylindrical symmetry, so that two refractive indices are sufficient for their characterization, namely n_{\parallel} for light polarized parallel to the fiber direction and n_{\perp} for light polarized perpendicularly to the fiber direction. The determination of birefringence, $\Delta n = (n_{\parallel} - n_{\perp})$, usually involves measurement of optical retardation, $\delta = (2\pi d/\lambda)\Delta n$, and of the fiber diameter, d . The light scattering technique gives a good measure of fiber diameters of various PBT samples. This technique involves an analysis of the forward-scattered radiation patterns produced when the fiber is placed in a collimated laser beam. Preliminary efforts have been made to measure the optical retardation in PBT fibers using the compensating techniques (Berek compensator, Babinet compensator).

The Becke-Line Method was also applied to determine the refractive indices n_{\parallel} and n_{\perp} and birefringence Δn of PBT fibers. In this method, PBT fiber is placed in a series of immersion liquids of different refractive index and examined under a polarizing microscope. Under these conditions, a thin band of light (called the Becke line) is seen at the edge of the fiber sample. Under the microscope, the narrow bright band moves toward the medium of higher refractive index if the focus is lowered. Since the plane of incident light can be adjusted parallel or perpendicular to the stretch direction of fibers,

it is possible to determine $n_{||}$ and n_{\perp} separately. However, the PBT fibers examined had both refractive indices greater than the refractive index of diiodomethane (1.740), which is the highest value known in any single liquid. Special high refractive index liquids (to $n = 2.2$) are on order.

3.5 Theoretical Calculation of PBT Refractive Index

The refractive index (n) for the isotropic polymer can be calculated from group contributions of various chemical bonds, using the following three different relationships between n and molar refraction R :

(a) the Lorentz-Lorenz Equation

$$R_{LL} = \frac{(n^2 - 1)}{(n^2 + 2)} \cdot V \quad (3.1)$$

(b) the Gladstone and Dale Relation

$$R_{GD} = (n - 1) \cdot V \quad (3.2)$$

(c) The formula due to Vogel

$$R_V = n \cdot M \quad (3.3)$$

where M is the molecular weight and V is the molar volume of the repeat unit of the polymer (10).

Assuming the additivity of group contributions to molar volume and molar refraction and that the polymer is in an isotropic state, the refractive index of PBT was calculated from the three different relations discussed above.

<u>Approach</u>	<u>Calculated Isotropic Refractive Index</u>
Lorentz-Lorenz	1.865
Gladstone-Dale	1.836
Vogel	1.785

Calculations of the fiber refractive indices, $n_{||}$ and n_{\perp} , and birefringence, Δn , were made using the relationship between molecular refraction and polarizability:

$$\frac{4}{3} \pi N \alpha_i = \frac{(n_i^2 - 1)}{(n_i^2 + 2)} V, \text{ where } i = \parallel \text{ or } \perp \quad (3.4)$$

$$\frac{4}{3} \pi N \alpha_i = \frac{(n_i^2 - 1)}{(n_i^2 + 2)} \frac{M}{\rho} \quad (3.5)$$

where α_i is the polarizability of the (polymer) molecule in the direction i , n_i represents the refractive index in the direction i , N is Avogadro's Number, and ρ is density. The molecular polarizability, α , can be calculated from the summation of the polarizability contributions of all individual chemical bonds making the structural repeat unit:

$$\alpha_{\parallel} = \sum b_L \cos^2 \theta + \sum b_L \sin^2 \theta \quad (3.6)$$

$$\alpha_{\perp} = \frac{1}{2} \left[\sum b_L \sin^2 \theta + \sum b_T (1 + \cos^2 \theta) \right] \quad (3.7)$$

where θ is the angle between the bond and the direction in question, b_L is the polarizability along the bond, and b_T is the polarizability across the bond.

The calculations give for the highly oriented PBT filaments the following values (with $\rho = 1.6$):

$$n_{\parallel} = 2.147$$

$$n_{\perp} = 1.679$$

$$\Delta n = (n_{\parallel} - n_{\perp}) = 0.47$$

$$n_{iso} = \frac{1}{3} (n_{\parallel} + 2n_{\perp}) = 1.835$$

Note that these estimates do not include any internal field effects, which may be significant.

3.6 X-Ray Diffraction of Fibers

Wide-angle x-ray photographs of PPTA, PBO and PBT have been taken using the standard Laue technique, employing normal film as well as a polaroid intensifier-cassette. It was found possible to cut down the exposure times by a factor of two with use of the polaroid cassette. However, the polaroid film was found to be unsuitable for weaker reflections and is therefore useful only for a quick screening of polymer samples and not for obtaining quantitative estimates of intensities.

The flat-film XRD (x-ray diffraction) photographs of both PBO and PBT indicate a high degree of orientation but a general lack of well-defined reflections located on layer lines which generally characterize three-dimensional lattices. Reciprocal lattice photography has been carried out using a Buerger Precession X-Ray Camera. Zero-level photographs were obtained using two different geometries: (a) fibers parallel to x-ray beam, and (b) fibers normal to x-ray beam.

Initial zero-level precession photographs of PBT fiber (see Figure 3.2) suggested scattering by parallel arrays of periodic cylinders. The scattering distribution expected from such an array was calculated in cooperation with Visiting Professor L.V. Azároff⁽¹¹⁾. The model consists of parallel chains of period \underline{c} , free to assume any relative orientation about the chain axis and any relative displacement $\delta \underline{c}$ along the chain axis. Assuming further that the lengths of the chains ($N\underline{c}$) are quite large compared to differences in individual chain lengths, the scattered intensity is given by:

$$\langle I_s \rangle = I_e N^2 F^2 \sum_m \sum_{m'} J_0(kr_{mm'}) \langle \exp[2\pi i \ell (\delta_m - \delta_{m'})] \rangle$$

where $J_0(kr_{mm'})$ is the zero-order Bessel function obtained by averaging

the interchain vector r_{mm} , over all orientations from 0 to π ,

k is the scattering vector,

I_e is the intensity scattered by a single electron,

F is the structure factor of the repeat units of length c .

Note that for $\ell = 0$, i.e., in the equatorial plane, $\langle I_s \rangle$ is given by a series of Bessel functions evaluated for each possible interchain separation and weighted by the number of such pairs. If one further assumes a hexagonal array of (7) cylindrically symmetric chains spaced a distance (a) apart, $\langle I_s \rangle$ for $\ell = 0$ is given by

$$\langle I_s \rangle = I_e N^2 F^2 [7 + 24J_0'(ka) + 12J_0(\sqrt{3}ka) + 6J_0(2ka)] \quad (3.9)$$

Assuming such a hexagonal packing of cylinders leads to a calculated density of only 0.9 g/cc. Further x-ray and electron diffraction work has shown the fibers contain more ordered regions in addition to a solid nematic phase. Present results indeed indicate PBT fibers consist mostly of ordered crystalline material with a minor amount of a solid nematic phase.

3.7 Radiation Damage

PBO and PBT exhibit good electron beam (100 KV, room temperature) radiation resistance. A Faraday cup and Keithley electrometer were employed to measure beam currents and the decay of diffraction peaks were estimated visually from diffraction patterns. As is normal for fibers, chain axis reflections (00 ℓ -type) are more resistant. The most susceptible reflections are those of the smallest d_{hkl} . The dose for decay to 50% of the initial diffracted intensity for PBO, PBT and PPTA (Kevlar) is on the order of 3 coul/cm² compared to 1×10^{-2} coul/cm² for polyethylene (see Table 3.3).

3.8 Electron Diffraction

By placing a fiber in a suitable high surface tension liquid and pricking the fiber with fine needles under a stereoviewing microscope, longitudinal sections of fibers thin enough for transmission electron microscopy may be obtained by surface tension aided microfibril dispersion. The longitudinal sections of fibers obtained by splitting were examined by wide angle electron diffraction (WAED) and bright and dark field images of fibrillar bundles were recorded.

The WAED patterns confirm the general features observed in XRD patterns. However, unlike XRD patterns, the WAED patterns vary in nature, depending upon the particular region (which is a fraction of a micron) under examination. The XRD pattern represents an overall average of fiber structure.

Electron diffraction patterns were obtained from different regions of the fibrillar fragments. A variation in mesomorphic lattice order from one site to another within the same sample was found (see Figure 3.3). The diffraction patterns obtained showed a transition from liquid crystalline order (Figure 3.3A) to three-dimensional order (Figure 3.3B), indicative of the different degrees of order encountered in a given fiber. Analysis of the most ordered patterns was most instructive. In addition to the very high number of equidistant meridional streaks (up to 20 orders being observable on the negatives), which correspond to a fiber repeat of 12.35 \AA , the equatorial reflections are well resolved, and indicate the following spacings*:

*The letters following each distance have their usual meaning for the relative observed intensities.

5.83 S	1.82 M-V
3.54 VS	(1.75) VW
3.16 M	1.71 W
(2.96) VW	

PBT samples 53-46, 53-47, 53-50 and 53-55 (all Carnegie-Mellon fibers) have been extensively investigated by electron diffraction and dark field microscopy techniques. These four samples give mostly highly ordered (crystalline) diffraction patterns with many (00 l) orders on the meridian. From the observed eight equatorial reflections and the fiber repeat, two probable unit cells are proposed (see Figure 3.4):

Cell I Monoclinic

$$a' = 5.83 \text{ \AA}$$

$$b' = 3.54 \text{ \AA}$$

$$c' = 12.35 \text{ \AA}$$

$$\gamma = 96^\circ$$

$$Z = 1$$

Cell II Monoclinic

$$a = 7.10 \text{ \AA}$$

$$b = 6.65 \text{ \AA}$$

$$c = 12.35 \text{ \AA}$$

$$\gamma = 63^\circ$$

$$Z = 2$$

Unit cell I corresponds to a very simple arrangement of parallel sheets (Figure 3.5) whereas Unit cell II (same figure) would allow more possibilities. Both unit cells have of course the same calculated density of 1.69, which closely matches the observed density of approximately 1.6 for a fiber without macroscopic voids. The value of the fiber repeat corresponds exactly to the length of the repeat unit⁽¹²⁾ Confirmation of the monoclinic packing, setting angle and choice between the two cells may be possible with more highly ordered fibers obtained from heat treatment. Nevertheless, the present packing already allows a very reasonable interpretation of the different

electron diffraction patterns.

If we assume a nearly planar molecular conformation^{*}, the PBT "crystallite" may be schematically shown as in Figure 3.5 (an all-parallel packing is taken for simplicity). The schematic emphasizes the two-dimensional character of this ordering, which explains essential features of the diffraction patterns. Small random translations of the chains along their axes causes the loss of all non-equatorial reflections as observed for example in Figure 3.3A. Such disorder may be typical of rigid rod systems. It has already been observed for example, from nematic fibers of poly- γ -benzyl-L-glutamate and certain aramid fibers⁽¹³⁾. As compared to this last case, the translational freedom of PBT molecules is enhanced by the absence of hydrogen bonding. Diffraction patterns as in Figure 3.3A can be considered to arise from crystallites of smaller lateral extent with more complete translational freedom along the chain axes. The number of meridional streaks is unaffected by the extent of this disorder, as it derives from the rigidity of the molecules.

Application of the Scherrer equation to the equatorial electron diffraction reflections would give the average size of the crystallites. Dark field imaging, which gives the actual size distribution, is preferred.

These electron diffraction data differ from the earlier hexagonal close packing of rods suggested by the nematic like x-ray pattern of fiber 53-46. The better instrumental resolution of the electron diffraction patterns shows that the broad equatorial spots actually consist of several individual

^{*}In the crystal structure of the model compound⁽¹²⁾, the angle between the two moieties of the repeat unit is 23°.

reflections*. The calculated unit cell density of 1.69 is now much more in line with the measured value of approximately 1.6. Further work is necessary to decide between cell I and cell II and to eventually determine the detailed molecular structure.

3.9 Analysis of the Broadening of 00 ℓ Electron Diffraction Lines

Electron diffraction patterns of PBT depict a series of disc-shaped maxima on the meridian. Since several orders of diffraction are available, it is possible to separate the effects of finite crystallite size and lattice distortion from an analysis of line breadth vs the order of diffraction.

In order to perform a line-profile analysis on the relatively sharp 00 ℓ discs or streaks, it is necessary to minimize the instrumental contribution to the observed line-broadening. This was accomplished by minimizing the divergence of the incident electron beam by means of a small condenser aperture. The WAED pattern of PBT #27554-9-5 (Celanese) was recorded using highly coherent illumination with an exposure time of five minutes. The influence of radiation damage on the width of 00 ℓ reflections is negligible at this dose.

Samples of PBT suitable for electron diffraction studies were prepared by the peeling technique, without recourse to ultrasonication.

Profiles of 00 ℓ diffraction lines were obtained by measurement of optical densities on the meridian of the flat film pattern, employing a Joyce-Loebl Microdensitometer. The profile of the strong 00 ℓ peak could

*A recent flat film x-ray photograph of fiber 53-46 by Dr. D. Wiff of UDRI (see Figure 3.6) using an evacuated sample-film holder, agrees well with the present electron diffraction findings. However, the less ordered regions in the fibers may well correspond to the nematic packing model.

not be recorded since this reflection was engulfed by the direct beam. Profiles of the 00ℓ reflections up to the twelfth order were recorded. The relative peak intensities of various 00ℓ reflections are compared in Table 3.4. The positions of 00ℓ maxima were obtained by using evaporated gold for calibration.

Angle-dependent corrections (e.g., Lorentz and absorption corrections) could be ignored in the present case due to very low values of 2θ and the thinness of the sample. The background has a slope and a curvature to it, hence a smooth background line was drawn by joining the low-angle and high-angle tails of the profiles. The area under the profiles was measured after eliminating the background and the integral breadths for various diffraction profiles were estimated. These values are listed in Table 3.5.

The line-profiles of 00ℓ reflections have a Cauchy shape. Such a line shape is theoretically predicted for a fibrous polymer containing a size-distribution of paracrystallites. Support of this inference comes from a plot of integral breadth $\delta\beta$ against ℓ^2 (Figure 3.7), which is linear within experimental limits of error. Theoretical calculations for an "ideal paracrystal" show that the integral breadth is given by (14):

$$\delta\beta_{00\ell} = \frac{1}{\bar{L}} + \frac{\pi^2 g^2 \ell^2}{\bar{c}} \quad (3.10)$$

where \bar{c} is the average spacing between the reflecting (00ℓ) planes, $g = \Delta c/\bar{c}$ is the coefficient of variation of the fiber repeat distance, \bar{L} is the weight-average dimension of paracrystallites and ℓ is the reflection index or the order of reflection. Equation (3.10) permits a separation of finite crystal size and lattice distortion influences on 00ℓ . Accordingly, the slope of $\delta\beta_{00\ell}$ vs ℓ^2 plot gives $\pi^2 g^2 / \bar{c}$, (hence g)

and the intercept on the ordinate gives $1/\bar{L}$ (hence \bar{L}). In the present case, we obtain a value of 150 Å for the (weight-) average length of "para"-crystallites and a g-value of 3%.

Vainshtein⁽¹⁵⁾ suggests the interaction radius of a paracrystalline lattice is (inversely) related to the degree of disorder of g. That is, the average size of the coherently diffracting domains is inversely proportional to g. Theoretical considerations show that $g\sqrt{L/c}$ is a dimensionless parameter which can be considered as a constant (α) for all paracrystalline materials.

For PBT a value of $\alpha = 0.1$ is obtained from the present data. This value agrees well with the value of α ($= 0.08$) obtained for native and regenerated cellulose, another class of stiff chain polymers⁽¹⁶⁾. (Derivatives of cellulose can be spun from liquid crystalline solutions.)

The value of 150 Å for crystallite length in PBT corresponds well with the crystallite size of similar magnitude observed in the dark field electron micrographs of PBT fibers (see Section 3.12).

3.10 Small Angle X-Ray Scattering of Fibers

Small angle patterns were recorded employing a pinhole vacuum camera using Ni filtered CuK_α radiation. The small angle scattering from PBT is rather weak and shows diffuse void scattering confined mainly to the equator. The pattern is similar to the void scattering seen in PPTA by Johnson and coworkers⁽¹⁷⁾ but is much less intense.

3.11 Electron Microscopy

A JEOL 100 CX electron microscope, operated at 100 kV, was used throughout this work. To prepare thin specimens, fibers were repeatedly peeled into

small fragments with the aid of sharp needles, while immersed in water. The fibrillar fragments were then directly picked up on carbon coated grids. In some cases, the suspension was mildly sonicated to aid in dispersal of the fragments.

Dark field (DF) imaging was performed with the tilted beam technique, the reflection selected by a 6×10^{-3} rad. objective aperture. All pictures were recorded on Kodak SO-163 films, with maximum magnification (DF) of 10,000X.

Preparation of the fibers for electron microscopy is illustrated in Figure 3.8 which shows the image (scanning electron microscopy) of a partially peeled fiber. The internal fibrillar structure is quite apparent. Repeated splitting gives fragments suitable for transmission electron microscopy. Small fibrils of variable width, down to a cross section of circa 70 Å, are observed in some regions. Electron diffraction patterns were easily recorded from such highly oriented fibrillar bundles.

3.12 Dark Field Electron Microscopy

All dark field images below have been obtained from the strongest equatorial reflection ($d = 3.54 \text{ \AA}$). Dark field images obtained from patterns similar to the one shown in Figure 3.3A do not exhibit high contrast. Figure 3.9 is such a DF image obtained from patterns similar to the pattern in Figure 3.3A. Small crystallites are regularly distributed throughout the fragment. Such features are comparable to other observations on certain PPTA fibers⁽¹⁸⁾ or PE fibers⁽¹⁹⁾. The strongest diffracting crystallites are elongated in shape with their average length being about five times larger than their width, which ranges from approximately 60 to 80 Å. The more numerous,

smaller crystallites are difficult to distinguish from the background, due to inelastic scattering. Figure 3.10 associates the bright field (BF) and DF images of a peeled and mildly sonicated fragment. A very marked banding transverse to the fiber direction appears in the DF image. This observation, again, is comparable to what has been seen in PPTA fibers⁽¹⁸⁾. In the thinner part of the fragment, the banding is regular, and each transverse dark band, 200 Å in width, makes an angle of about 70° with the fiber direction. The periodicity of the banding is of about 1200 Å, as compared to 5000 Å for PPTA fibers⁽¹⁸⁾.

Each of the flat ribbons appears to consist of smaller "microfibrils" of lateral dimensions varying from 50 to 80 Å as previously mentioned. These ribbons exhibit a wavy texture, each microfibril changing its direction in register with its neighbors. The corresponding DF image shows a characteristic banding associated with the BF image "waves". The size of well defined crystallites in the DF image is about 50 x 500 Å but a great number of smaller crystallites is also noted. Their long direction makes a slight angle (10° to 20°) with the fiber direction, similar to that made by the microfibrils in the corresponding parts of the BF image. The contrast between dark and bright zones depends on the sharpness of the kinks. As inelastic scattering is small because of the thinness of the ribbons, the grey background is mainly due here to diffuse scattering from less ordered regions.

This last observation suggests that orientation conditions, instead of noncrystalline zones, are responsible for the observation of the dark zones. This is further demonstrated in Figure 3.11, which shows an "s-shaped" fiber. As the fiber progressively changes its orientation, the small zones (A) reverse their contrast from dark to bright, and conversely for the large zones (B). Therefore, textured ordered regions are present all along the

ribbon, with neighboring crystallites in approximately the same orientation within a band. The banding period here varies from 1000 to 2000 Å. A double system of banding is also noted (see region C in Figure 3.11).

From the above observations, a schematic of the texture of these kinked ribbons is proposed in Figure 3.12. The ribbon is built up of closely packed microfibrils, well apparent in the kink zones. Each microfibril consists of a succession of narrow crystallites embedded in a somewhat less ordered matrix. The left hand portion of the schematic illustrates the banding observed in the DF image. Whether the bands appear due to the fragmentation of the fibers during the sample preparation, or on the contrary, are characteristic of the as-spun fibers, is not known at present. The non-linear stress-strain behavior and the elongation at break (3%) suggest the bands may be shear bands.

3.13 Structure of Coagulated Films

The morphology of PBO and PBT which had been coagulated from dilute solution in MSA has been investigated. The effects of coagulant composition and post-neutralization with NH_4OH have been considered and the stability of the polymers to the electron beam have been assessed.

Samples have been prepared by two methods. In the first method, the polymer solution was sheared onto a glass slide which is then placed into the selected coagulant. The resultant thin film was then picked up on a gold microscope grid. If the sample was to be neutralized, the sample grid was floated in a 10% NH_4OH bath for two hours followed by a distilled water bath for five hours. After air drying the specimens were observed in the electron microscope. Gold grids were required because the standard copper grids were attacked by MSA.

The second method of sample preparation involved dropping the solution

into the coagulant, dispersing by ultrasound and placing a drop of the resultant suspension onto a support grid.

PBO-25613-354 (IV = 1.8) was observed to form a randomly oriented, fibrillar, polycrystalline mat when coagulated in methanol from a 0.05 wt % solution in MSA. The mat was comprised of fibrils approximately 200 Å in diameter (see Figure 3.13) which are reminiscent of PPTA fibrils observed by Takahashi⁽²⁰⁾. The interplanar d-spacings are insensitive to subsequent neutralization at this concentration and molecular weight.

PBO-2122-72 (IV = 18) was observed to form polycrystalline, fibrillar mats when coagulated into selected H₂O/MSA and CH₃OH/MSA mixtures from a 0.11 wt % solution in MSA. These films appeared thicker than those observed for PBO. The PBT films retained some of the orientation induced during preparation (see Figure 3.14) as evidenced by texturing in the electron diffraction patterns. Presumably, this is due to the higher viscosity and hence longer relaxation time of the PBT solution compared to the PBO solution. The d-spacings were relatively insensitive to coagulation composition but proved to be sensitive to post neutralization.

Film samples are easily prepared which are thin enough for study by electron microscopy. This requires a minimum amount of time and allows screening of coagulant baths. Furthermore, crystalline films with varying degrees of orientation have been obtained.

TABLE 3.1: DEFECTS IN PBT-27554-#

Fiber #	Contained Voids	Linear Number Density (Defects/mm)	
		Erupted Voids	Circumferential Bonds
6-2	0.5	15	14
6-3	0.6	15	7
9-1	0.4	<1	7
9-3	1.1	<1	26
9-5	0.2	<1	1
9-6	0	4	8
9-7	0.1	5	9
9-10	0.7	7	9
9-11	0.8	3	5

TABLE 3.2: FIBER DIAMETER

Fiber	Diameter (μ)	S.D. (μ)
# 6-1	39.6	4.7
# 6-2	23.1	1.6
# 6-3	25.0	1.05
# 9-1	25.1	0.65
# 9-3	23.2	0.54
# 9-6	25.8	0.86
# 9-7	22.5	0.98
# 9-10	23.1	1.11
# 9-11	26.1	1.3

TABLE 3.3: RADIATION RESISTANCE OF SELECTED POLYMERS

Room Temperature, 100 KV, $j_{\text{PBT}} = 6.3 \times 10^{-2} \frac{\text{amp}}{\text{cm}^2}$, $j_{\text{PBO}} = 1.4 \times 10^{-2} \frac{\text{amp}}{\text{cm}^2}$

Doses for 50% Decay of Initial Diffracted Intensity

<u>PBO</u>		<u>PBT</u>	
<u>d(Å)</u>	<u>(coul/cm²)</u>	<u>d(Å)</u>	<u>(coul/cm²)</u>
1.07	1.3	0.77	3.0
1.18	1.3	1.11	3.0
1.33	1.3	1.19	4.5
1.80	0.26	1.23	-
1.97	7.6	1.27	4.5
2.38	7.6	1.46	3.5
3.52	1.9	1.64	2.3
5.65	7.6	1.89	2.3
		2.14	-
		2.58	17.1
		2.60	14.7
		3.71	-
		4.36	-
<u>PPTA (Kevlar)</u>		<u>Polyethylene</u>	
<u>d(Å)</u>	<u>(coul/cm²)</u>	<u>d(Å)</u>	<u>(coul/cm²)</u>
4.33	0.2	4.10	0.01
6.45	3.0		

TABLE 3.4: RELATIVE INTENSITIES OF 00 l REFLECTIONS

<u>Reflection</u>	<u>Relative Peak Intensity</u>
001	--
002	0
003	85
004	0
005	100
006	72
007	0
008	18
009	25
0010	31
0011	20
0012	8

TABLE 3.5: INTEGRAL LINE BREADTHS FOR 00 l REFLECTIONS

<u>Reflection</u>	<u>Integral Breadth</u> <u>δ_{00l}^B (\AA^{-1})</u>
003	0.012
005	0.019
006	0.026

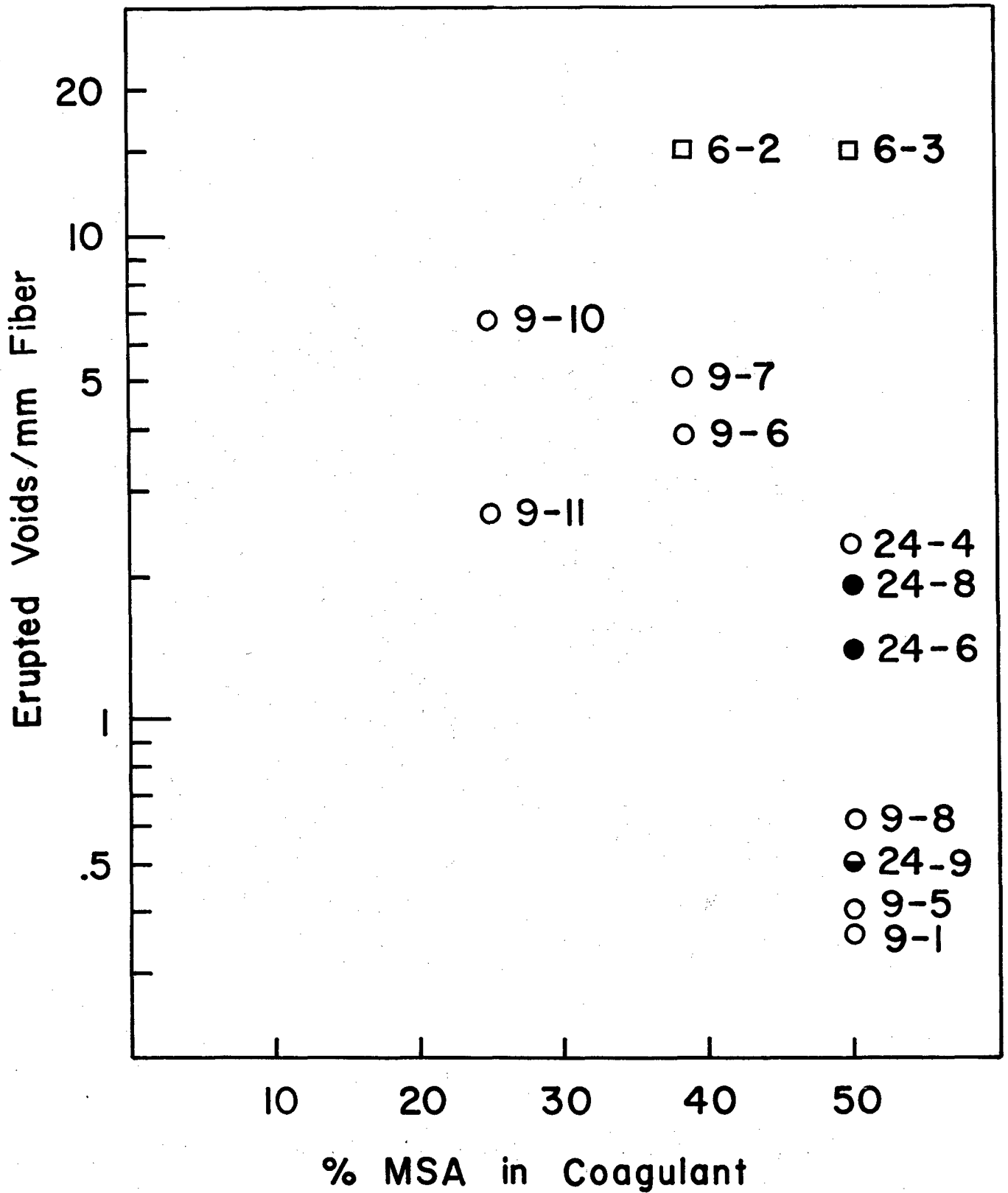


Figure 3.1: % MSA in Coagulant.

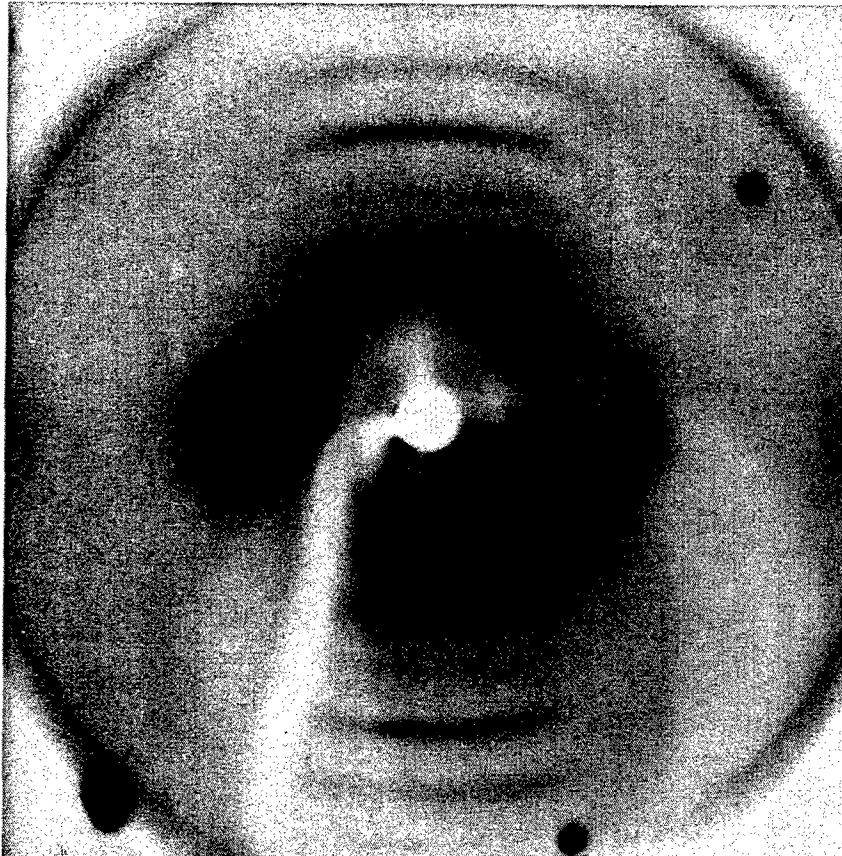
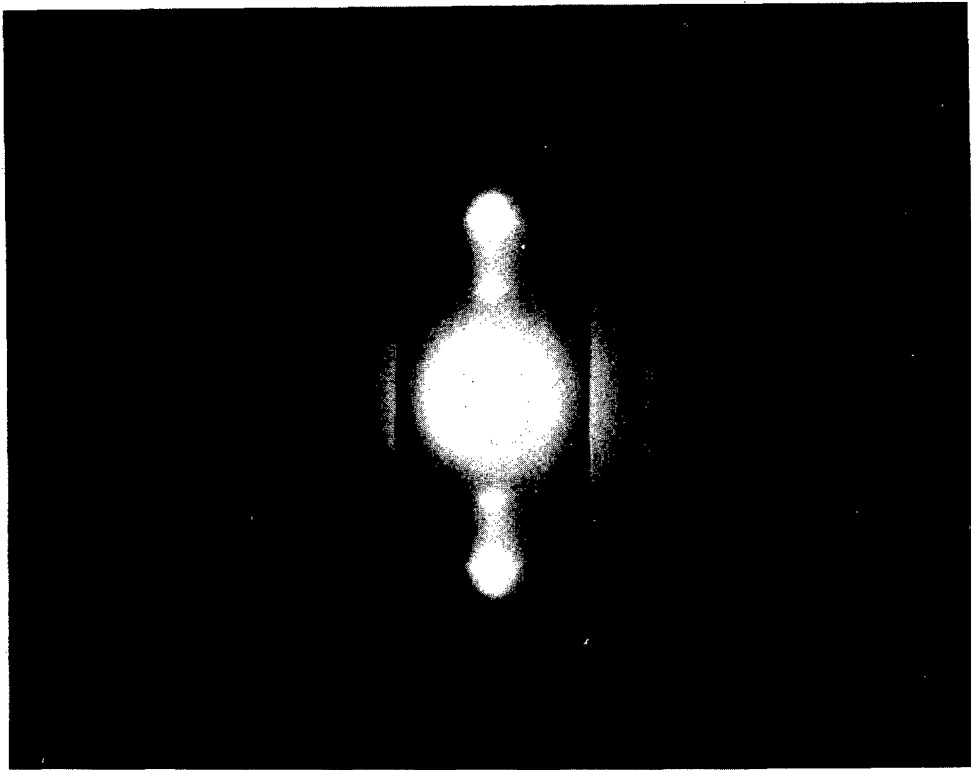


Figure 3.2: Zero level precession x-ray photograph of PBT (CHU 53-46). Fiber Axis Vertical

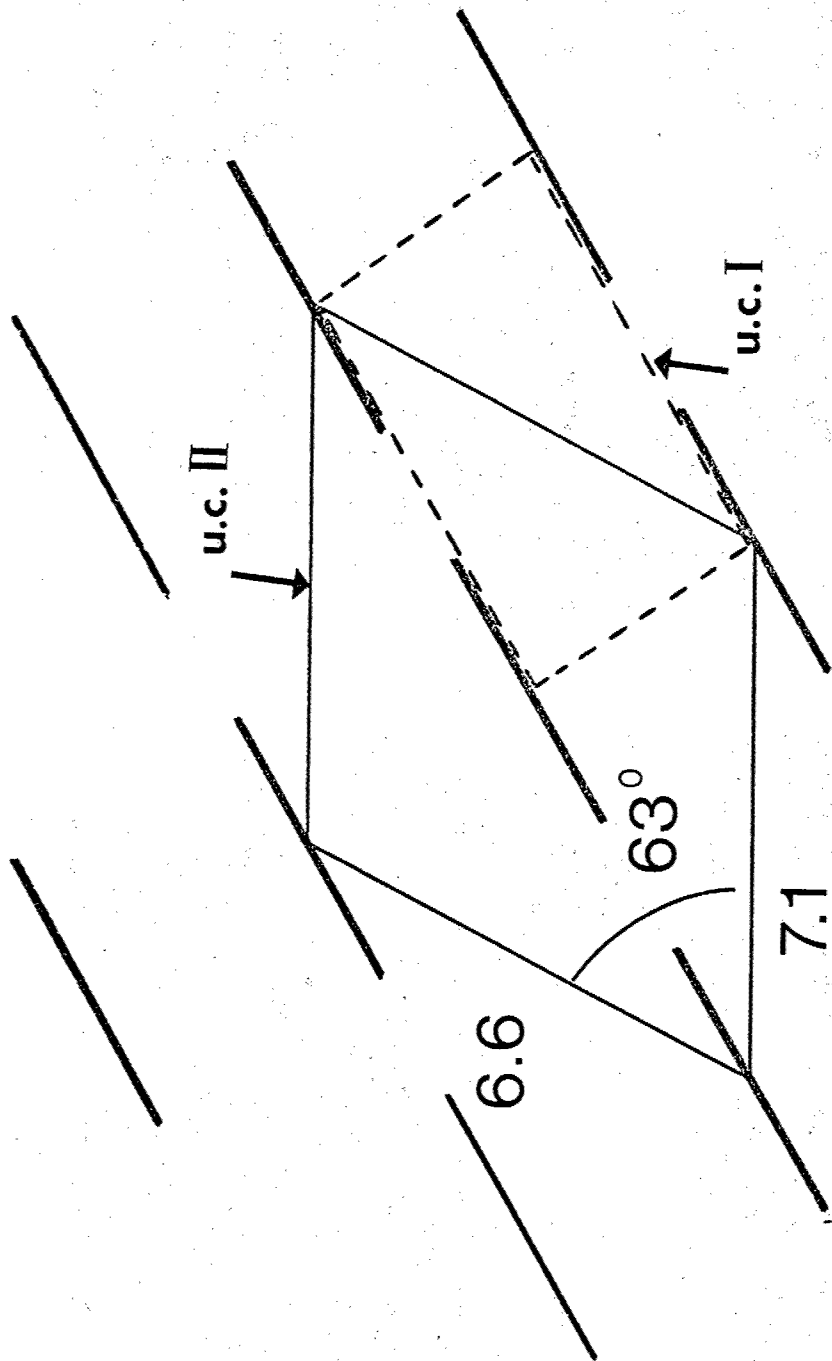


(a)



(b)

Figure 3.3: Electron diffraction patterns from fibrillar fragments of a PBT fiber exhibiting different degrees of order.



$$C = 12.35$$

Figure 3.4: Possible unit cells of the PBT crystal structure (projection down the \vec{c} axis).

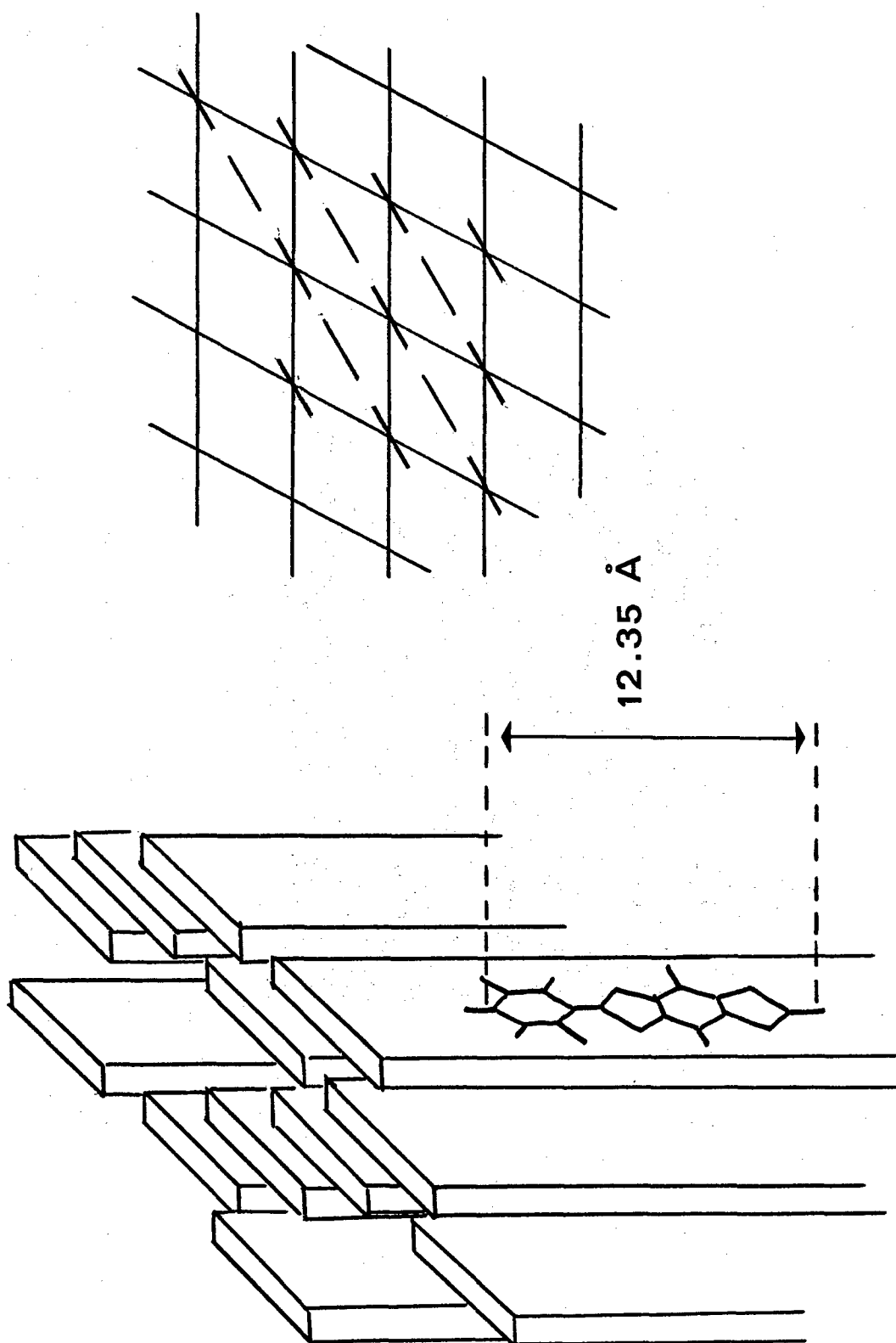


Figure 3.5: Schematic of the proposed arrangement of PBT molecules in a crystallite.



Figure 3.6: Flat Film X-ray of Fiber 53-46
(courtesy of Dr. D. Wiff, UDRI).

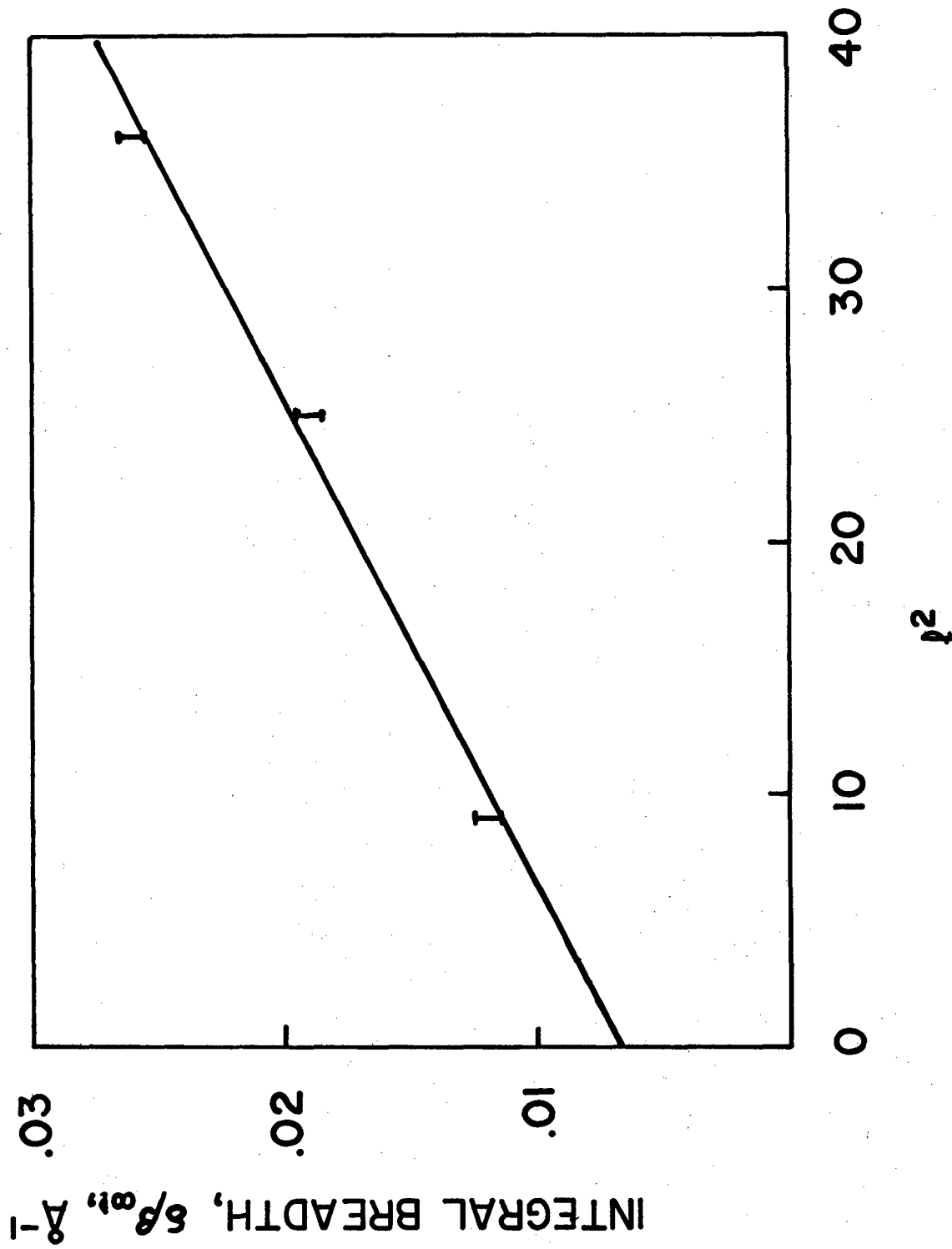
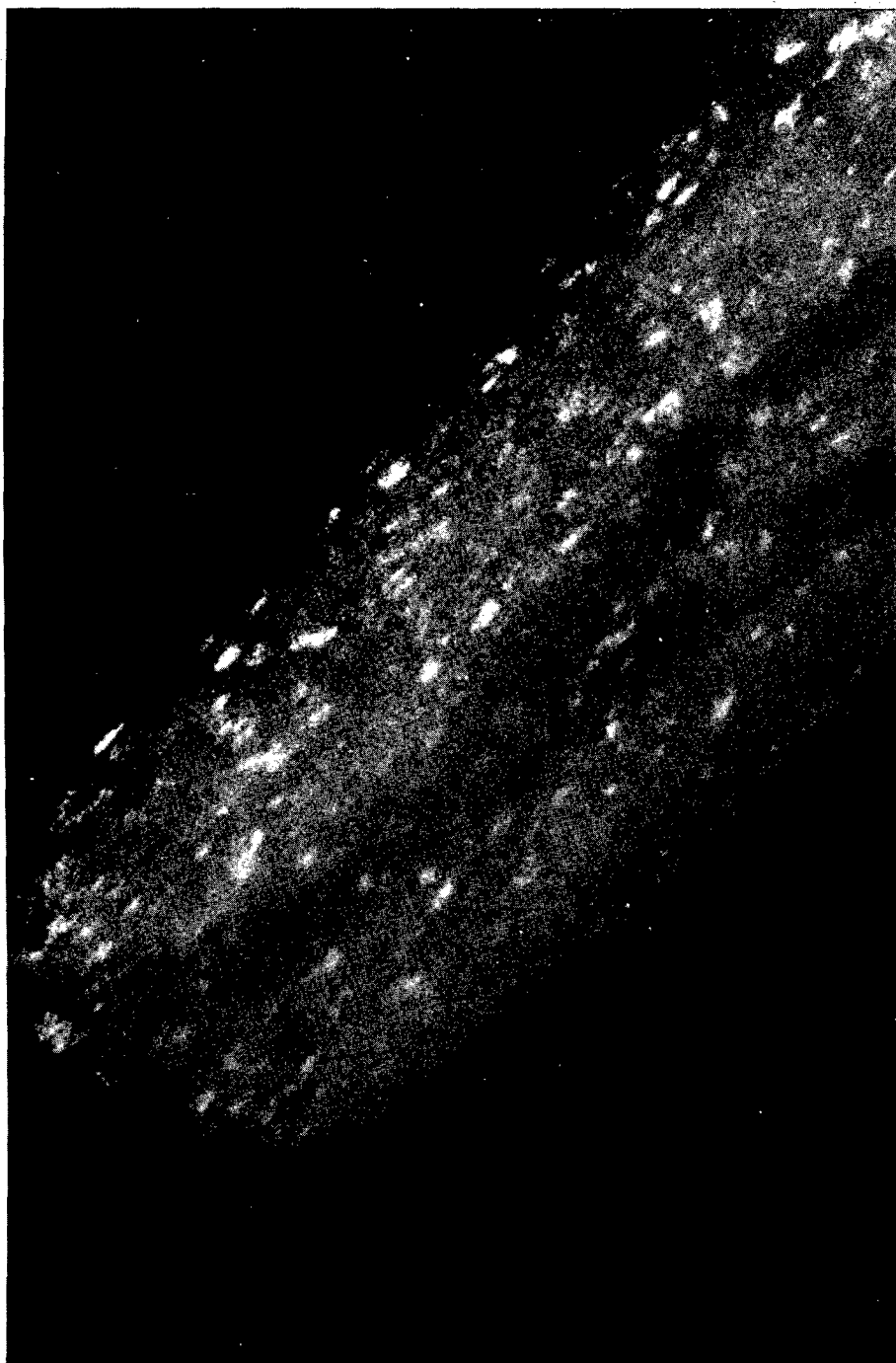


Figure 3.7: Plot of Integral Breadth $\delta\beta$ against the Square of the Order of Reflection.



10μm

Figure 3.8: Scanning electron micrograph of a partially peeled PBT fiber.



100nm

Figure 3.9: Equatorial dark field image of a fragment of a PBT fiber.



.5 μm

Figure 3.10: BF (left) and DF (right) images of ribbon-like fragments of a PBT fiber showing the fibrillar texture of the ribbons.



·5 μm

Figure 3.11: Electron micrograph showing orientation effects on the banded structure.

.1 - .2 μm

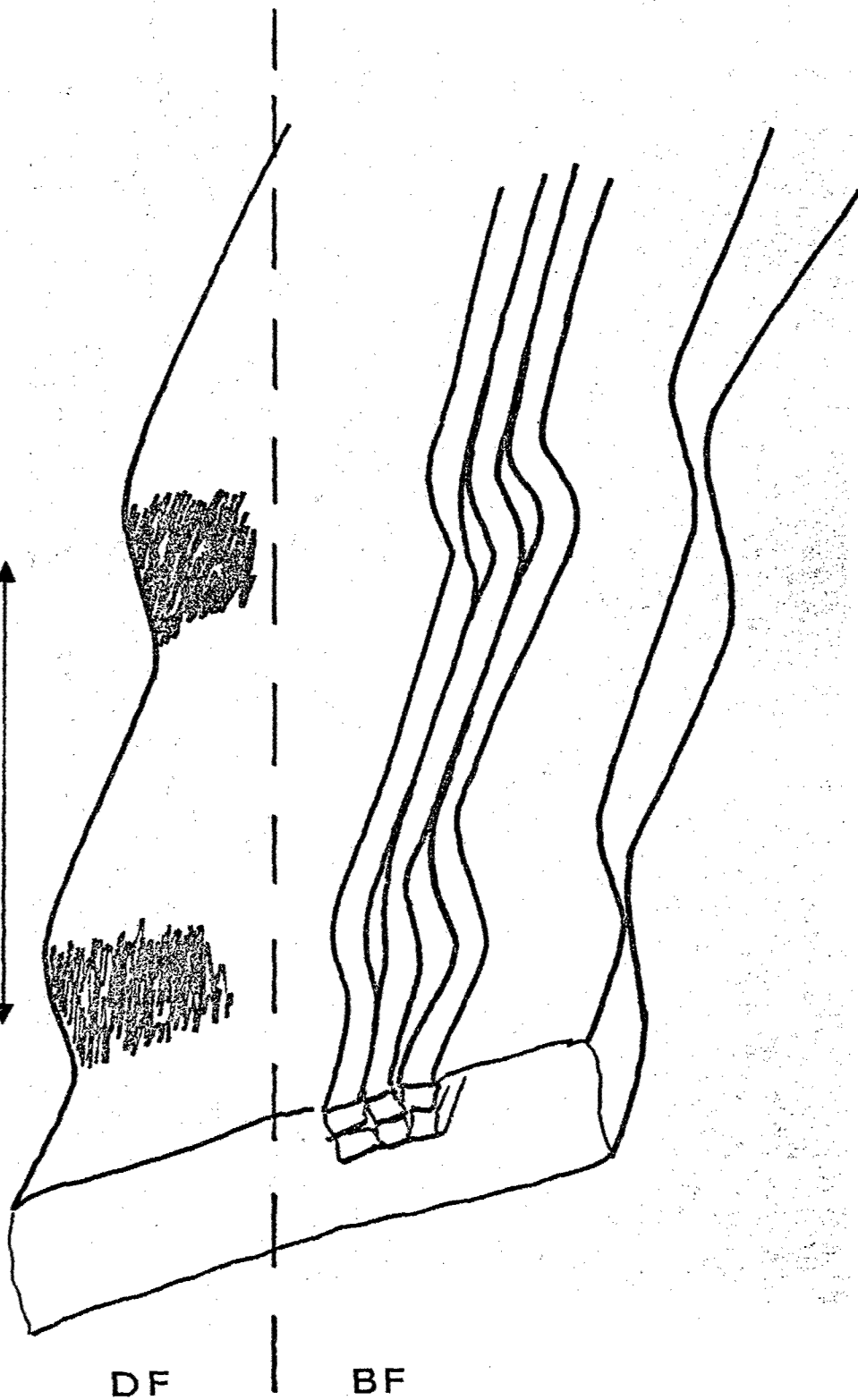


Figure 3.12: Schematic of the fibrillar structure of the ribbon-like fragments obtained after peeling and mild sonication of PBT fibers.

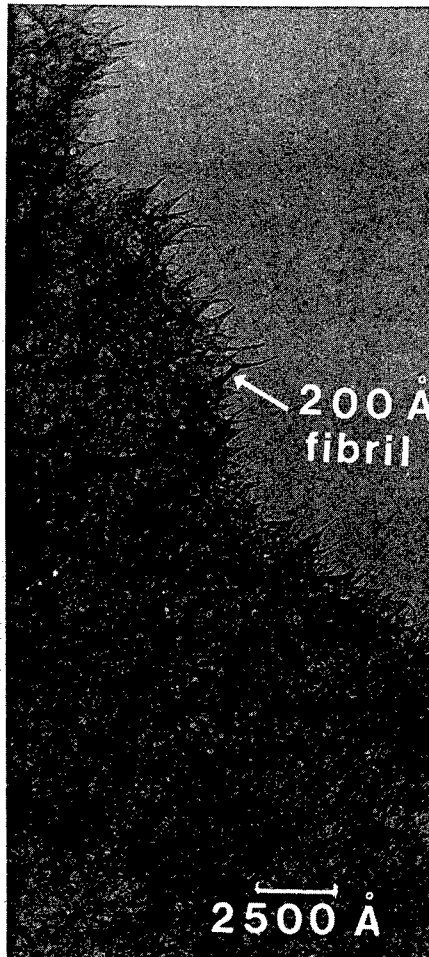
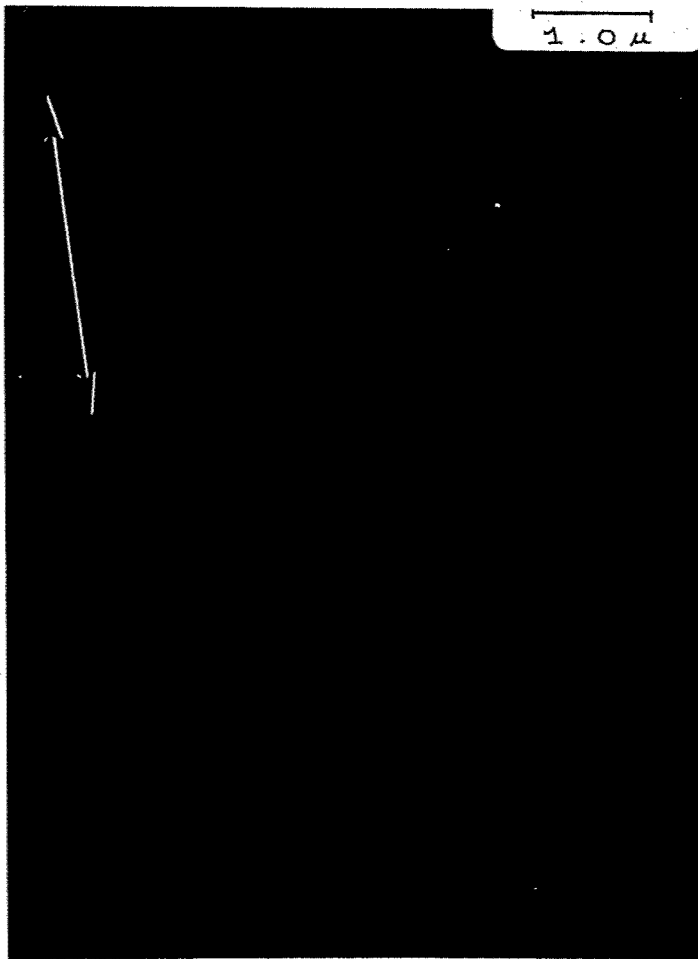
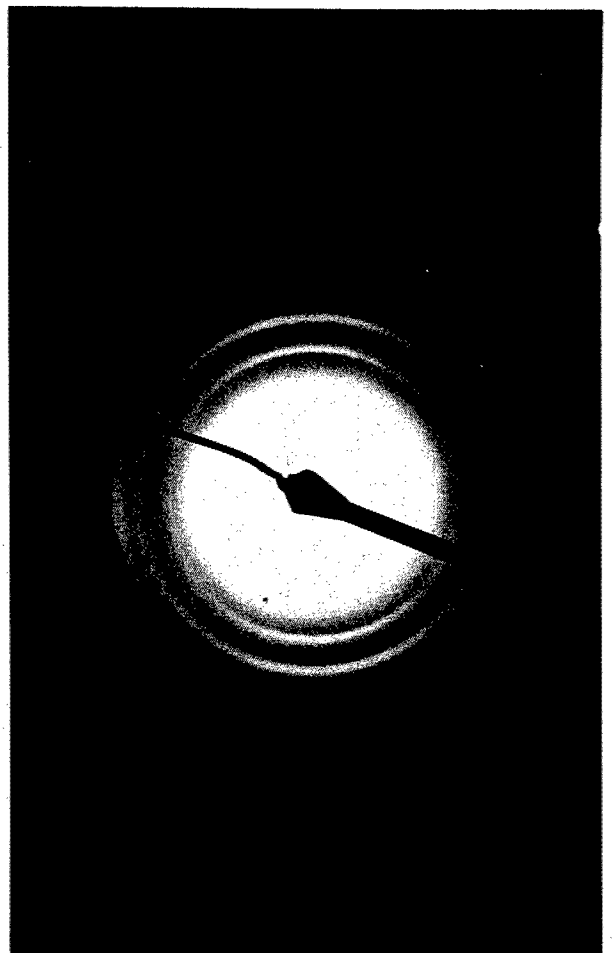


Figure 3.13: Bright Field TEM Micrograph of PBO Coagulated in Methanol at Room Temperature.



Bright Field



Electron Diffraction

Figure 3.14: Oriented Film of PBT Coagulated from 100% H₂O.

SECTION 4: MECHANICAL PROPERTIES

4.1 Introduction

The mechanical properties of PBT fibers have been investigated as part of this program during the past year. The original purpose of our contracted research was to relate the mechanical properties to measures of the polymer morphology, such as the degree of orientation or the rigidity of the molecules. This task of structure-property relationships has not been possible since the limited amounts of polymer samples (fiber) received have had their properties dominated by large imperfections in the fiber cross-section. The most noticeable and probably the most significant fiber defects are large voids and circumferential bands (see Section 3.2). The fibers have very high modulus but relatively low strengths and prior to heat treatment they exhibit plastic characteristics. The low strengths are the result of the large imperfections which cause premature failure due to stress concentrations in the flawed regions. If the processing could be improved to yield a high quality fiber, then it is expected that PBT will have properties equivalent to or in excess of the duPont Kevlar 49 fiber. All data taken to date suggest that PBT fiber is very similar to Kevlar fiber in that it is a highly anisotropic fiber that has very high tensile modulus, low compression and shear strengths, low transverse and shear moduli, and the potential for very high tensile strength.

4.2 Comments on Fiber Defects

Voids, circumferential bands and surface depressions are most likely caused by the high shrinkage stresses that develop during the fiber coagulation process. In the central core of the fiber the stresses would have a large component of tension in both the radial and axial directions. Cavita-

tion could be caused by tensile failure of the partially coagulated fiber core. The skin of the fiber, to be in equilibrium, must be under large axial compressive stresses and because of the poor compressive characteristics of these highly anisotropic materials, compressive instabilities or buckling can result in circumferential bands (depressions). Although improvements in the spinning process should diminish these effects, it should be again pointed out that the fiber geometry and size also plays a major role in determining the magnitude of these stresses. Of all the fiber shapes, the solid circular cross-section is by far the most sensitive to nonhomogeneous shrinkage. Making fiber tubes, or fibers with triangular or flattened cross-sections should greatly reduce the magnitude of these shrinkage stresses for any given spinning technique. Such techniques, which have been suggested in the past but have not yet been tried, could perhaps produce high quality fibers with the existing processing technology for PBT. Until defect free fibers and films can be produced it will be impossible to determine the structure property relationships because the properties are being dominated by defects.

4.3 Gauge Length Study

Strength (force at break) of fiber PBT 9-5 was investigated as a function of gauge length. Optical microscopy investigations indicated an average distance between voids of 1.8 mm, the largest void spacing observed for the 9 series fibers. Tensile tests on 1 to 2 mm gauge length specimens would possibly provide strength data on no-void sections giving a better approximation of ultimate mechanical properties.

Average tenacity for large gauge length (>10 mm) PBT 9-5 fibers was eight grams per denier. One to two mm gauge length samples gave an average tenacity of 9 g/denier, 10.8 g/denier being the highest value recorded. SEM

examination of fracture surfaces indicated fractures were localized at voids as for the larger gauge length specimens. An optically screened no void sample of PBT 9-5 gave a tenacity of 17 grams per denier, indicating a high potential for these materials if defect free fibers could be produced.

4.4 Fiber Morphology Summary

Relatively large scale morphological characteristics of PBT fibers were investigated using scanning electron microscopy (SEM). Fibers received from Carnegie-Mellon University had diameters ranging from 18-50 microns with variations of about 10% over the measurements taken. Fibers received from Celanese Corporation had diameters ranging from 12-30 microns with variations of 4-8%.

Two main surface features of the PBT fibers were observed. The first is the appearance of circumferential bands perpendicular to the fiber axis (see Figure 4.1). These bands were more pronounced in the Carnegie-Mellon fibers and were somewhat regularly repeating (about 2-3 fiber diameters repeating distance). A rotation study of the Carnegie-Mellon (single filament spun) fibers indicated the bands were nonuniform over the circumference of the fiber. Closer examination suggested they may have arisen due to compression buckling of the fiber on the small diameter spools (14 mm diameter) on which they were wound. The buckling marks were observed to lie on the compressive side of the residual curvature. The bands on the Celanese fibers, spun as 5-10 filaments in a fiber bundle, however, appeared to have resulted from contact with and separation from the other filaments in the fiber bundle.

The second main surface feature was the presence of longitudinal depressions running parallel with the fiber axis (see Figure 4.2). The length of

these depressions, common to both Carnegie-Mellon and Celanese fibers, was on the order of 20 microns or more. These depressions were later found to be associated with a slight collapse of the fiber about internal voids as revealed by studies of fracture surfaces.

Fiber diameters were calculated from SEM images and by light scattering and together with fiber deniers supplied by the processors, the average fiber densities were calculated. The calculated densities are summarized in Table 4.1.

Comparison of these densities with an ideal density of 1.69 is a measure of the volume content of the voids. Fracture surface examination and examination of internal surfaces revealed by longitudinal splitting indicate the large voids occupy around 15% of the fiber cross-sectional area at a void. These fracture surface studies also have indicated the fiber to be of fibrillar structure with the central core of the fiber less ordered than outer regions.

4.5 Environmental Effects

Samples of PBT 9-10 fiber were placed in various liquid environments (Skelly F., Chloroform, dimethyl acetamide, sulfuric acid, nitric acid, acetone, and water) for periods of two hours, one day and eight days and their mechanical properties evaluated at atmospheric conditions after water rinsing. Except for the two acids, the environments did not significantly affect the fiber mechanical properties. The two acids, however, did affect mechanical properties and the effect was seen to have occurred during the first two hours, the mechanical properties evaluated after two and eight days being the same. The nitric acid environment reduced fiber modulus from 800 g/denier to 600 g/denier and reduced strength from 8.5 g/denier to 6 g/denier. The sulfuric acid environment was more severe, reducing the

modulus to 300-400 g/denier and strength to 4 g/denier. The environment also changed the fiber color from its characteristic deep red to a golden color.

4.6 Heat Treatment

Preliminary heat treatment studies have been carried out using fiber PBT 9-3. Fiber samples were placed unstressed in an air oven at temperatures up to 300°C. Fiber modulus and strength did not change as a result of unstressed heat treatment, however, strain at break (ϵ_b) or the amount of "plastic" strain did vary. Figure 4.3 indicates the effect of time of heat treatment on ϵ_b as a function of time. The strain at break is seen to decrease sharply, then level off and remain constant after approximately 15 minutes. The effect of higher temperatures was seen to be a further reduction in the amount of plastic deformation present, i.e., the higher the heat treating temperature the closer the stress-strain curve was to being purely elastic. Figure 4.4 illustrates the effect of heat treatment temperature on the stress-strain behavior.

A 3% weight loss was measured for a 240°C heat treatment indicating possible loss of residual solvent/coagulant. A heat treatment was performed in a vacuum oven with nitrogen purge to exclude the presence of atmospheric oxygen during the heat treating. This treatment done at 200°C did not give as large a decrease in ϵ_b as did an air oven at 200°C (Figure 4.5).

4.7 Tensile Properties

Tensile properties of PBT fibers were evaluated on a Toyo Tensilon model UTM-11 tensile tester. A random selection of single filaments were centerline mounted on special paper tabs by epoxy glue. The tabs were gripped so that the test specimen was aligned axially in the jaws of a constant-speed

movable-crosshead test machine. The filaments were then stressed to failure at a constant strain rate $\epsilon = 0.02 \text{ min}^{-1}$. (Tests were done at room conditions on 20 mm samples.)

The portion of the indicated elongation contributed by the load train system and the specimen gripping system was taken into account in accordance with the "Standard Test Method for Tensile Strength and Young's Modulus of High-Modulus Single-Filament Materials" (ASRM, D3379-75e). This system compliance was determined experimentally for a given combination of test machine conditions, grip system and mounted specimen. It was subtracted from the indicated elongation to yield true specimen elongation in the gauge length.

The results of the tension tests are summarized in Table 4.1, where

T_b = Tenacity at break = F/D (F -force at break, D -denier);

σ_b = Stress at break = force per unit cross-sectional area;

$E_0 = \left(\frac{dT}{d\epsilon}\right)_{\epsilon=0}$ = Modulus of elasticity in terms of unit linear density;

Y_m = Young's modulus;

ϵ_b = Strain at break.

Calculations of strength (σ_b) and Young's modulus (Y_m) were based on average fiber diameters obtained from scanning electron microscopy studies. The calculated fiber densities reported indicate the need for re-evaluation of fiber denier (values given are Celanese data).

The character of the force-elongation behavior was also investigated. The following observations were drawn:

1. The dependence of the tenacity on the strain is essentially non-linear (Figure 4.6).
2. There is no strain rate dependence of stress on strain over the range of strain rates: 1, 10, 100 ($\% \text{ min}^{-1}$), (Figure 4.7).

3. The character of deformation of these materials corresponds to a model of an elastic-plastic body with strain-hardening.

4. The modulus of elasticity is seen to increase with increasing plastic strain (see Figure 4.6), for example, PBT-53-48, $E(\epsilon_p=0) = 600 \text{ g/D}$, while $E(\epsilon_p=0.7\%) = 750 \text{ g/D}$.

4.8 Bending Properties

The fiber loop strength was determined at a range of loop curvatures for Celanese 27554-6-2 fiber. The axial strain in the bent portion of the fiber is composed of a bending component and an axial tensile component. This additional bending component of strain, in the case of brittle material (which is the case for PBT fiber: strain at break 2-3%), can lead to a detrimental effect during textile processing and also in the ultimate applications of the material. Assuming plane sections, the maximum bending component of the strain can be calculated by (see Figure 4.8).

$$\epsilon_{\text{loop}} = \frac{r}{R + r} \quad (4.1)$$

where r = fiber diameter, R = loop curvature diameter. This formula is valid only if the axial compression properties and the tension properties of the material are the same. Assuming that failure occurs when the strain is equal to the strain at break in tension- (ϵ_b) , we have:

$$\epsilon^*(F_1) = \epsilon_b - \frac{r}{R + r} \quad (4.2)$$

where $\epsilon^*(F_1)$ is the critical axial tensile component of the strain which depends on the applied load F (see Figure 4.8). It is easy to calculate from the stress-strain curve in tension the critical value of load corresponding to ϵ^* (see Figure 4.8). In this way the theoretical loop strength,

F_l as a function of the ratio $r/(R+r)$ is:

$$F_l = F(\epsilon_b - \frac{r}{R+r}) \quad (4.3)$$

The theoretical loop strength is equal to the tensile strength if $R \gg r$, decreases with increasing ratio $r/(R+r)$; and equals zero when $r/(R+r) = \epsilon_b$.

The fiber loop strength was determined by performing tensile tests on fibers wrapped around mandrels of various diameters; the fiber configuration in this test is illustrated in Figure 4.8. The fiber looped over itself (Figure 4.8) was the most extreme case of bending evaluated. The measured values of loop efficiency - the ratio of loop strength to the tension strength - F_l/F_b as a function of the ratio $r/(R+r)$ are plotted in Figure 4.9. Also plotted is the theoretical loop efficiency. As can be seen from Figure 4.9, the experimentally determined loop efficiency is higher than could be expected from the theoretical consideration, and even is finite up to $r/(R+r) = 50\%$.

Disagreement of theoretical and experimental determination of loop strength can be understood if the properties of the material in axial compression are not the same as in tension. Actually, as seen from the SEM investigations of fiber behavior in bending (see Figure 4.10), the failure begins on the inside (compression) surface, indicating that strength in axial compression is significantly lower than in tension. Such deformation leads to a redistribution of the strain field in the fiber cross section at the expense of the reduction of the effective fiber diameter and in this way leads to the reduction of the maximum strain caused by bending. In turn, this explains the increasing loop strength with the correction in fiber cross section.

PBT fiber with a low value of rupture strain in tension is not brittle in bending as would be expected. Furthermore, the fiber in a bent state is still capable of sustaining considerable tensile load up to $\epsilon_{loop} = 50\%$. This phenomenon is explained by the difference in fiber mechanical properties in axial compression and tension.

TABLE 4.1: MECHANICAL TEST DATA

Fiber #	Denier g	Diameter microns	Density g/cm ³	T _b g/Denier	δ_b 10 ⁻ N/m ²	E _o g/Denier	Y _m 10 ⁻ N/m ²	ϵ_b %
53-47	6.5	31	0.96	5.1	4.5	500	440	1.2
53-48	9.9	30	1.56	5.0	7.2	600	860	1.7
53-49	6.2	28	1.12	6.1	6.4	760	800	1.4
53-50	4.5	26	0.94	6.4	5.2	700	580	1.1
53-51	4.8	22	1.40	5.8	7.0	800	1010	1.2
53-53	5.9	28	1.06	6.5	6.4	650	650	1.9
53-55	5.1	18	2.23	5.0	10.2	730	1430	1.0
53-56	6.5	29	1.09	3.8	3.8	710	720	0.8
53-57	7.1	25	1.61	3.4	4.7	360	500	1.4
62-60	(30.5)	52	1.60	6.2	8.8	350	490	3.6
62-61	(28.1)	46	1.88	4.6	7.7	340	560	3.2
62-62	(13.8)	39	1.28	7.2	8.3	542	620	3.0
62-64	(17.7)	44	1.29	6.1	7.0	420	480	2.9
62-66	(14.0)	40	1.24	7.8	8.5	580	630	3.7
62-67	(13.3)	39	1.24	7.3	8.0	530	580	3.8
6-1	5.1	32+12	0.70	8.0	4.9	350	220	6.2
6-2	4.2	22	1.23	11.0	11.9	614	670	3.0
6-3	3.1	23	0.83	16.5	12.1	1260	930	3.3
9-1	5.4	25	1.22	10.2	11.0	920	980	2.6
9-3	5.3	23	1.42	8.7	10.9	860	1080	2.7
9-5	3.3	17	1.62	8.3	11.9	873	1240	2.1
9-6	6.5	26	1.36	8.6	10.0	705	850	3.0
9-7	5.2	23	1.39	7.9	9.7	828	1013	2.1
9-10	5.3	23	1.42	8.5	10.6	800	1000	2.8
9-11	6.3	26	1.32	8.4	9.8	704	775	2.9
4B	1.64	12.3	1.53	9.1	12.3	900	1220	2.6
8B	1.94	12.4	1.78	9.8	15.4	890	1440	2.5
Kevlar	1.4	12	1.44	23	30	940	1200	2.4

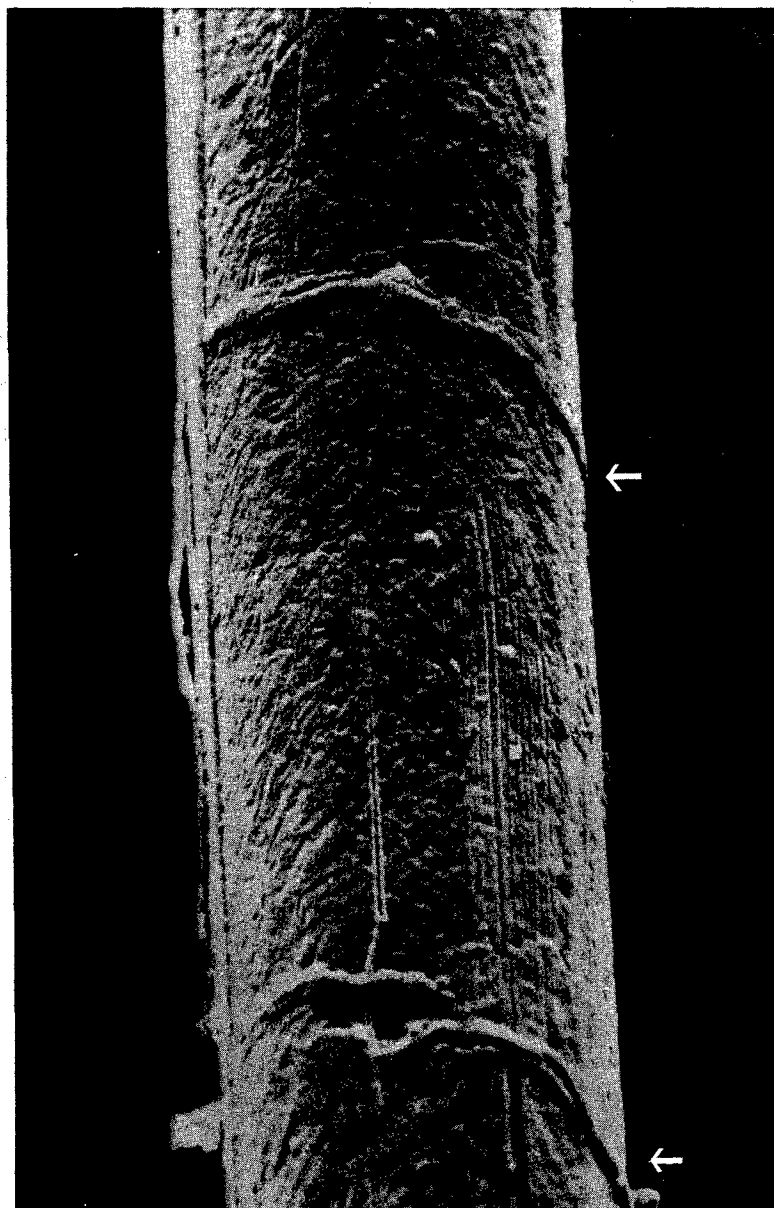


Figure 4.1: SEM Micrograph of a PBT 5348 Fiber. Arrows indicate characteristic circumferential bands.

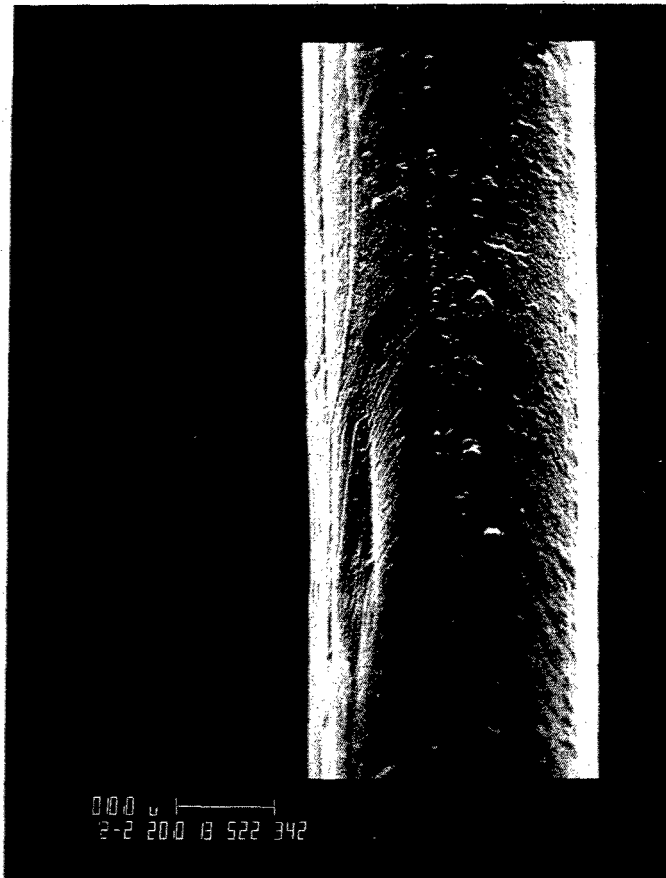


Figure 4.2: PBT 5348, SEM Micrograph Showing A Longitudinal Depression.

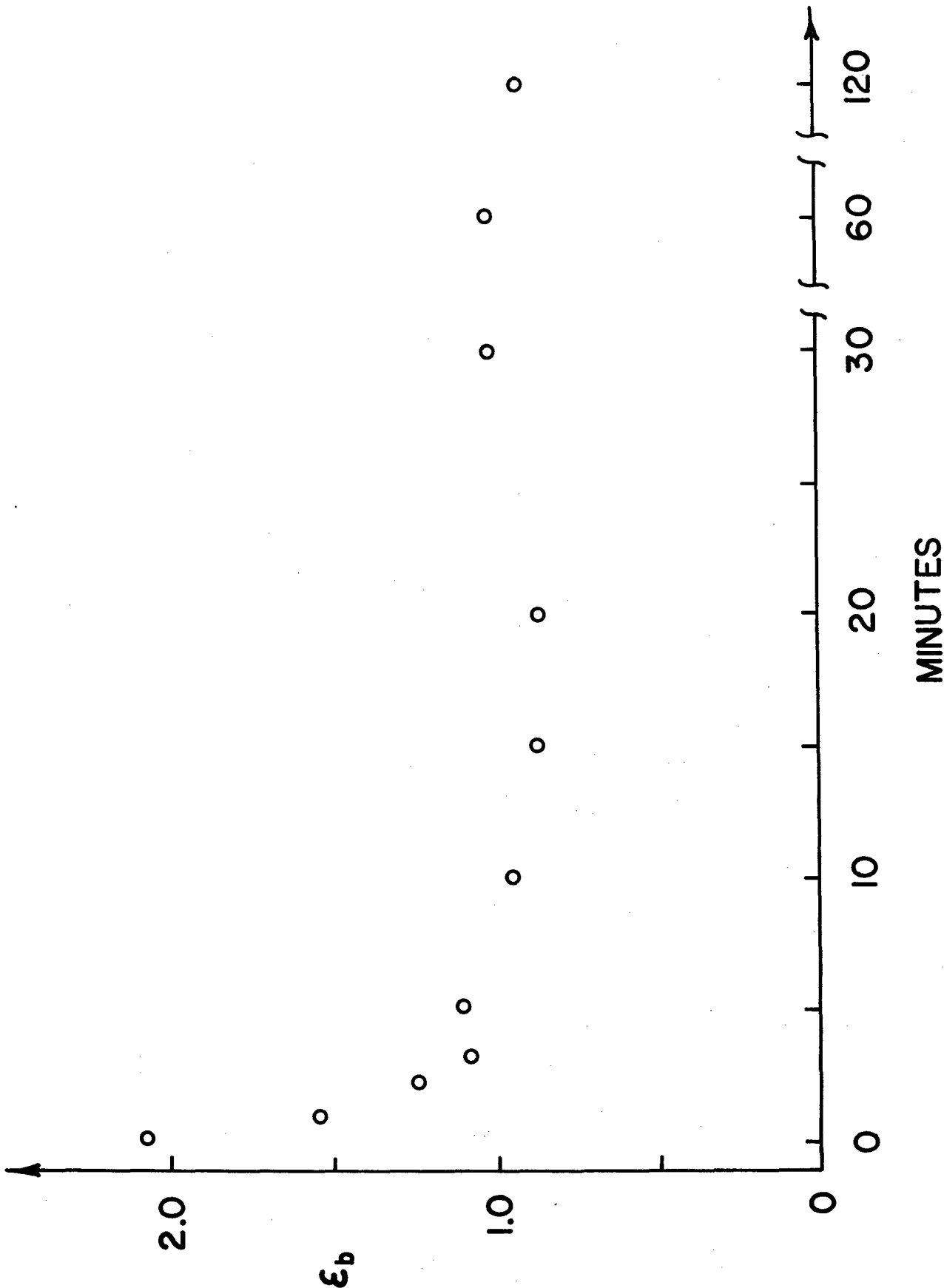


Figure 4.3: The Effect of Heat Treatment Time in a 175°C Oven on the Strain at Break of a PBT 9-3 Fiber.

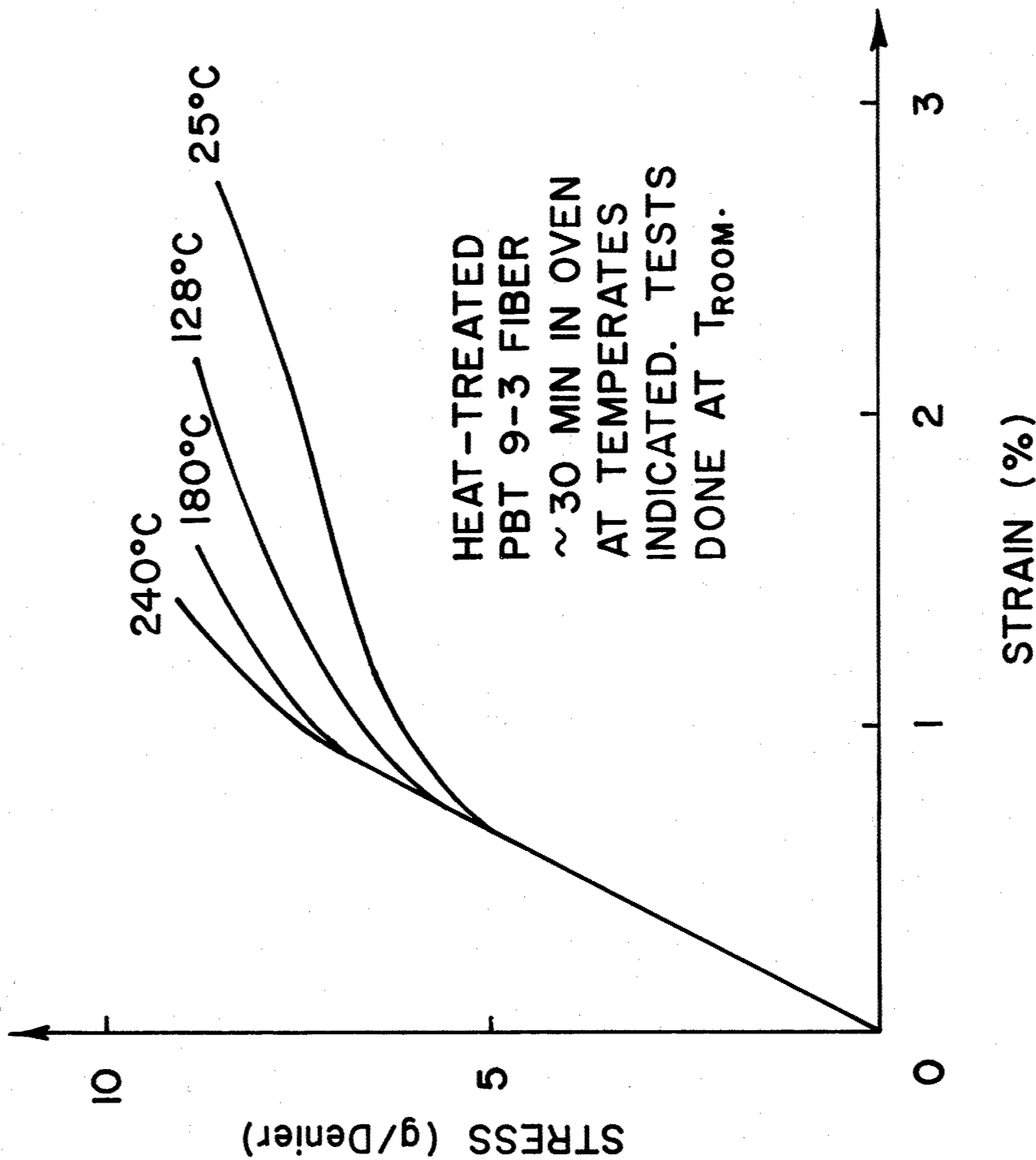


Figure 4.4: Effect of Heat Treatment Temperature on the Stress-Strain Curve of PBT Fiber.

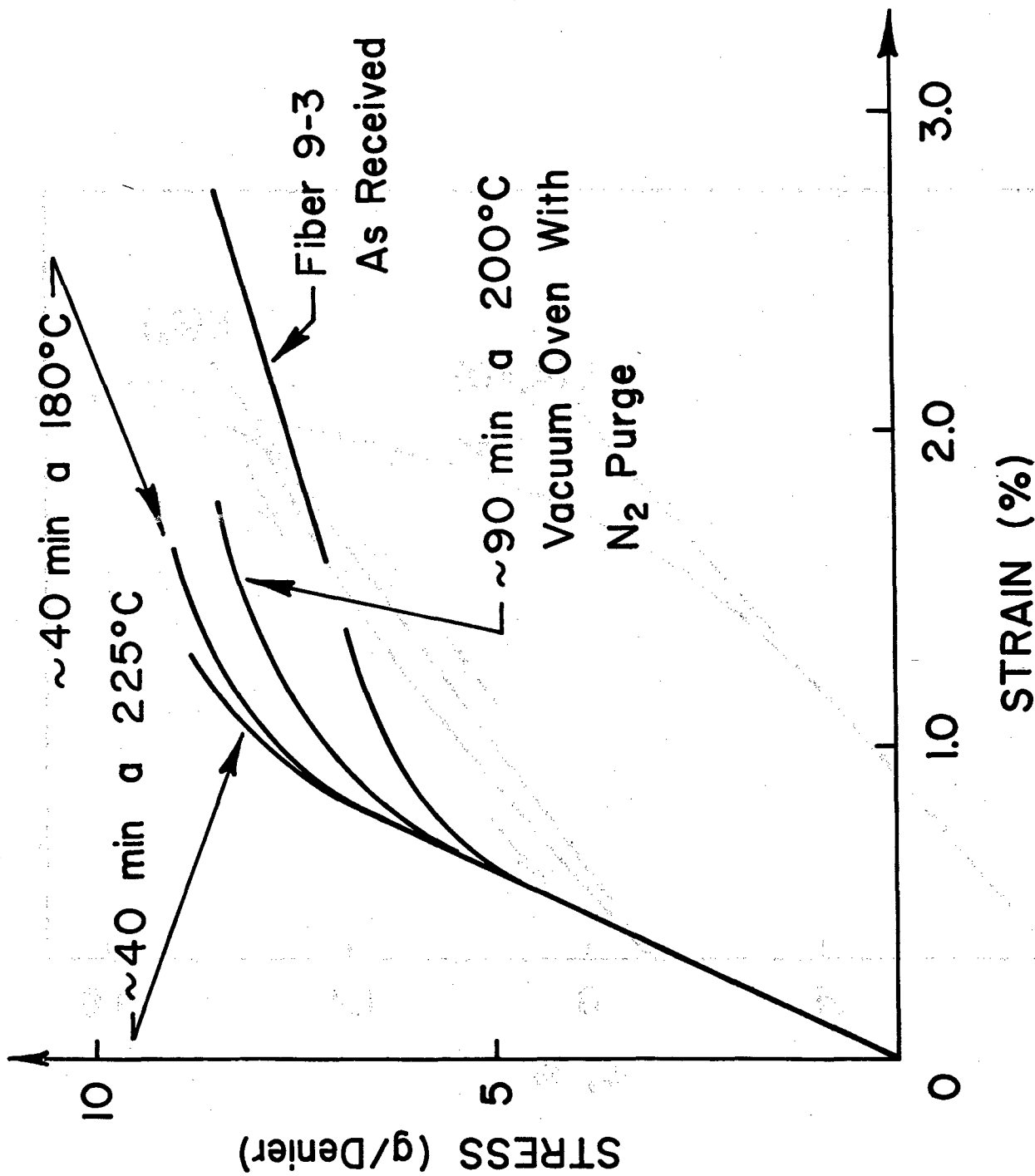


Figure 4.5: Comparison of the Stress-Strain Behavior of Fibers Heat Treated with and without Oxygen Present During Heat Treatment.

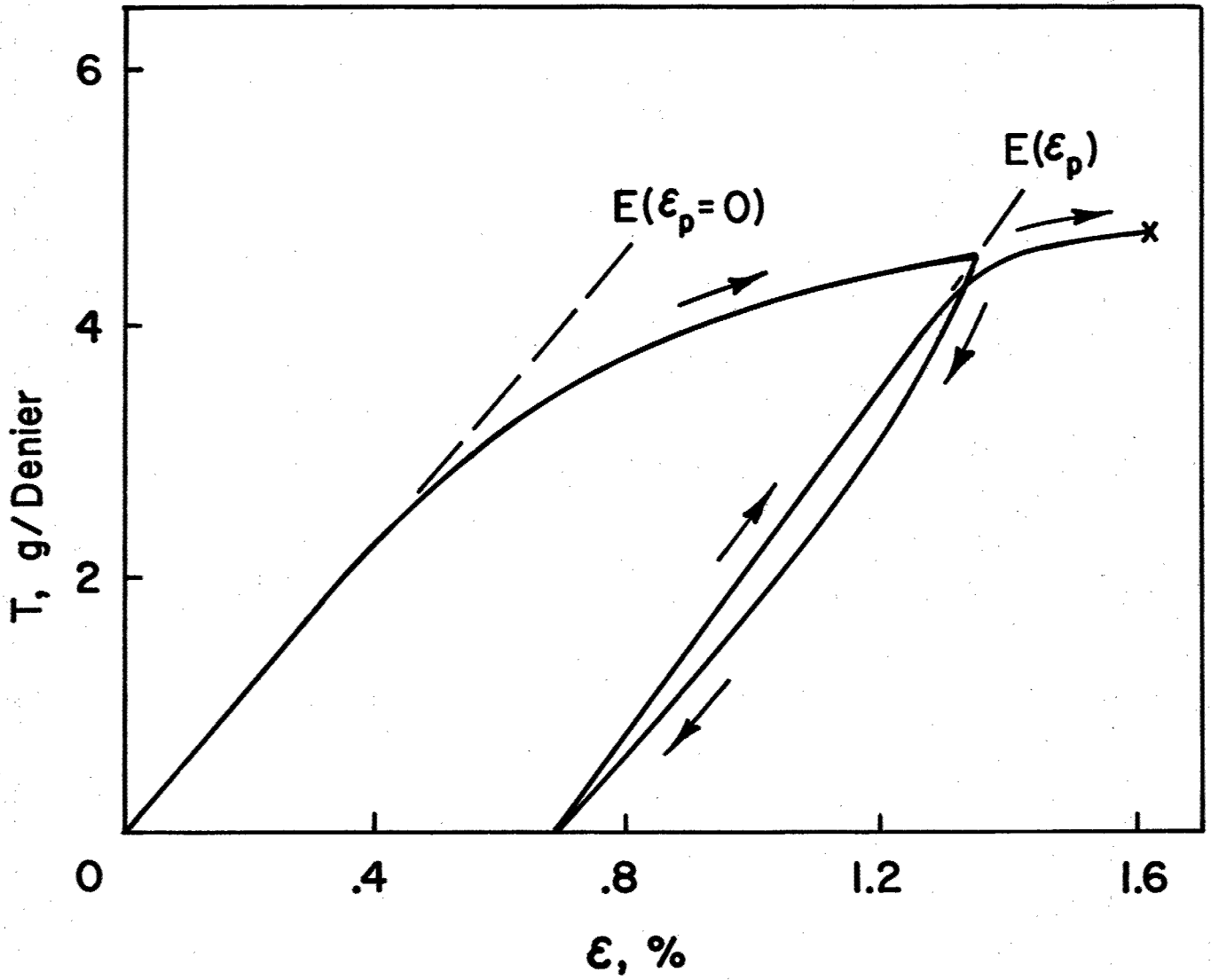


Figure 4.6: Tensile Behavior of PBT Fiber.

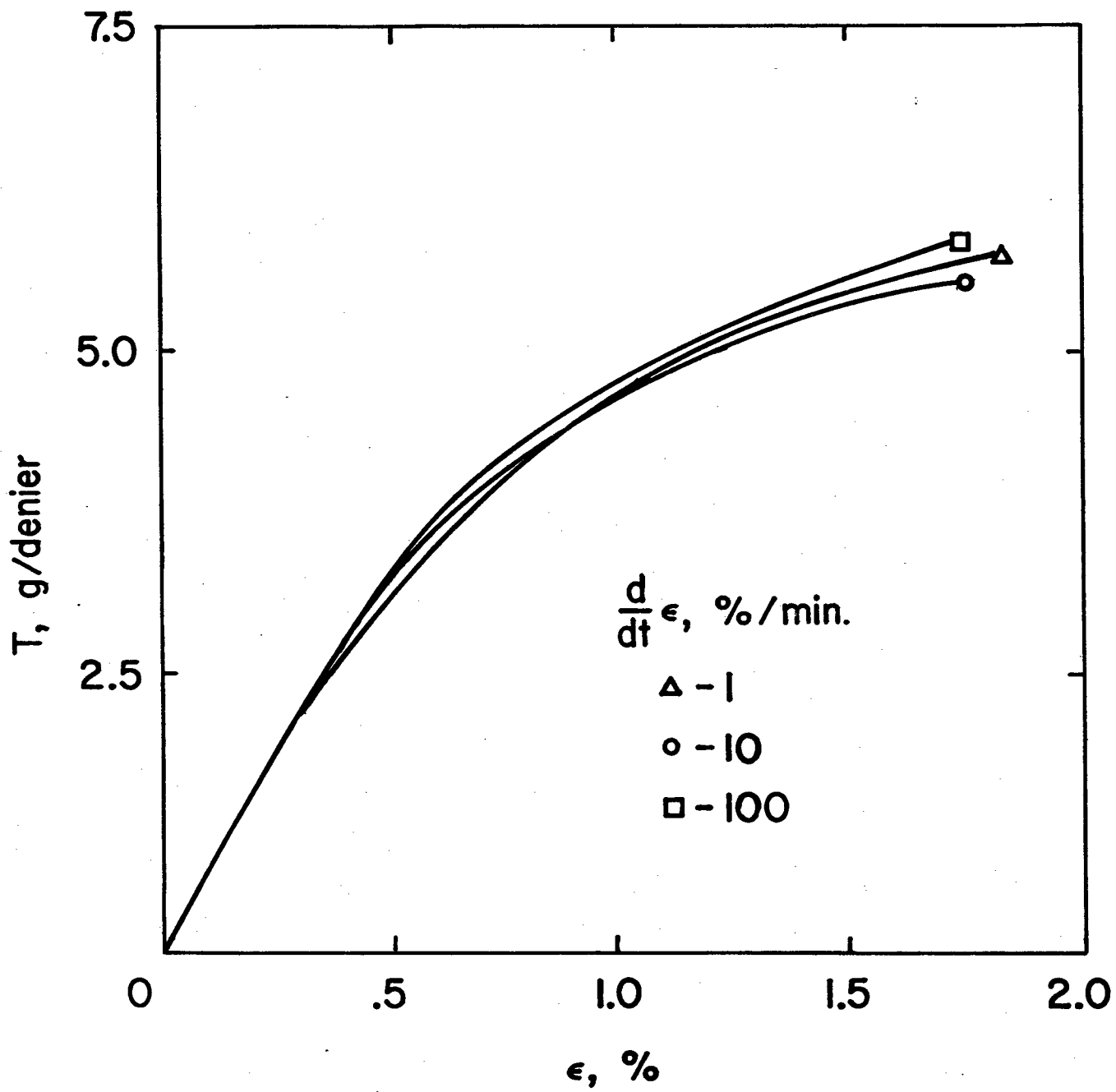


Figure 4.7: Strain rate independent behavior.

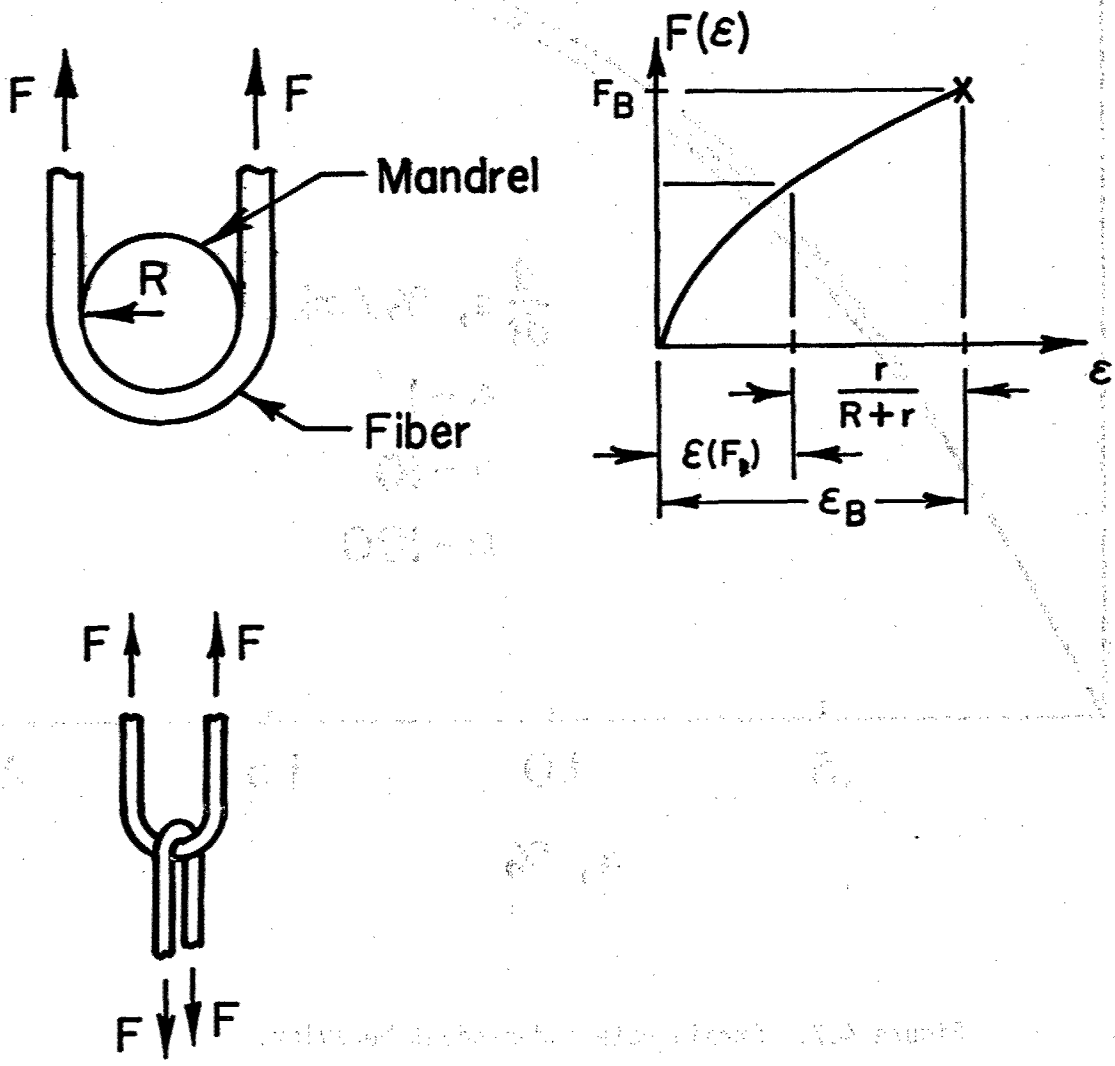
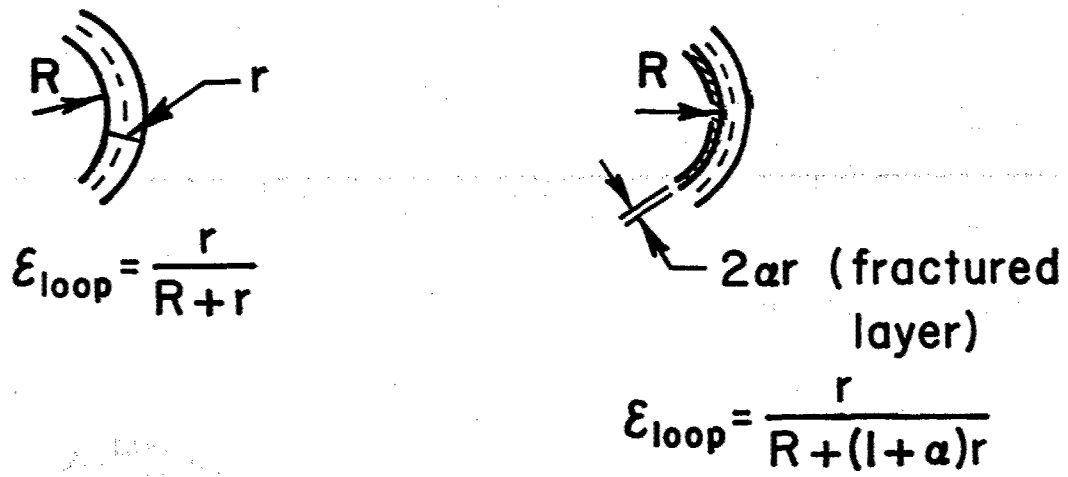


Figure 4.8 Analysis of Fiber Bending

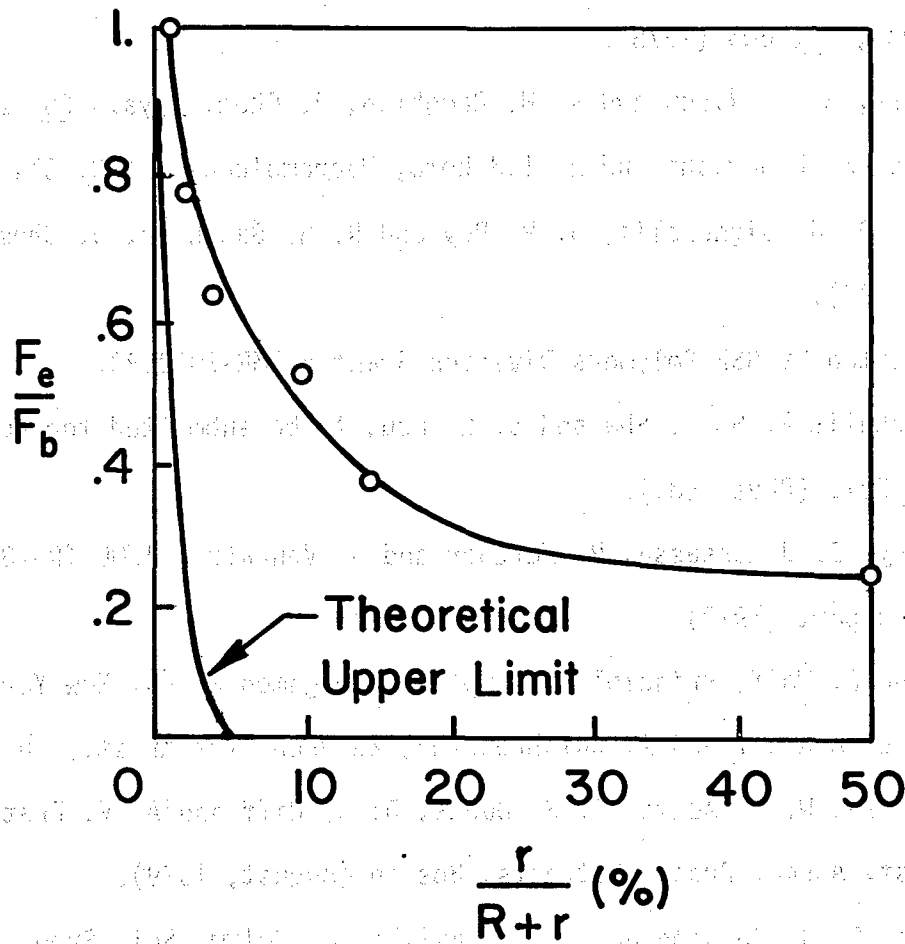


Figure 4.9: Fiber Loop Efficiency.

REFERENCES

1. L. Penn and F. Milanovich, *Polymer*, 20, 31 (1979).
2. D. Bloor, D. A. Fisher, D. N. Batchelder, R. Kennedy, A. C. Cottle, and W. F. Lewis, *Mol. Cryst. Liq. Cryst.*, 52, 83 (1979).
3. A. C. Cottle, W. F. Lewis, and D. N. Batchelder, *J. Phys. C: Solid State Phys.*, 11, 605 (1978).
4. V. K. Mitra, W. M. Risen and R. H. Baughman, *J. Chem. Phys.*, 66, 2731 (1977).
5. K. Tashiro, M. Kobayashi and H. Tadokoro, *Macromolecules*, 10, 314 (1977).
6. S. L. Hsu, A. J. Signorelli, G. P. Pey and R. H. Baughman, *J. Chem. Phys.*, 69, 106 (1978).
7. Work supported by NSF Polymers Division Grant # DMR-7902883.
8. D. J. Burchell, P. H. C. Shu and S. L. Hsu, to be submitted for publication, *J. Polym. Sci. (Phys. Ed.)*.
9. G. C. Berry, E. J. Casassa, P. Metzger and S. Venkatra, AFML-TR-78-164, Technical Report (1978).
10. M. Born and E. Wolf, *Principles of Optics*, Pergamon Press, New York (1959).
11. W. Adams, L. Azaroff and A. Kulshreshtha, *Zeitsch. fur Krist.*, in press.
12. M. W. Wellman, W. W. Adams, D. S. Dudes, D. R. Wiff and A. V. Fratini, *Amer. Cryst. Assoc. Proc. Abstracts*, Boston (August, 1979).
13. M. G. Dobb, D. J. Johnson and B. P. Saville, *J. Polym. Sci. Symp.*, 58, 217 (1977).
14. R. Hosemann and S. N. Bagchi, *Direct Analysis of Matter by Diffraction*, North Holland, Amsterdam (1962).
15. B. K. Vainshtein, *Structure Analysis by Electron Diffraction*, Pergamon Press, Oxford (1964).

16. J. Hasse, R. Hosemann and B. Renwanz, *Kolloid Z. u. Z. Polymer*, 251, 871 (1973).
17. M. G. Dobb, D. J. Johnson, A. Majeed and B. P. Saville, *Polymer*, 20, 1284 (1979).
18. M. G. Dobb, D. J. Johnson and B. P. Saville, *Inst. of Physics Conf. #36*, 403 (1977).
19. R. M. Gohil and J. Petermann, *J. Polym. Sci.(Phys.)*, 17, 525 (1979).
20. T. Takahashi, H. Iwamoto, K. Inove, and I. Tsujimoto, *J. Polym. Sci.(Phys.)*, 17, 115 (1979).